RECENT RESULTS FROM LEP

Joachim Mnich
CERN PPE-L3
CH-1211 Genève 23

Representing the LEP Collaborations

ABSTRACT

In this article, recent preliminary results of the four LEP experiments, ALEPH, DELPHI, L3, and OPAL, from running at energies above the Z resonance are presented. LEP was operated at center-of-mass energies between 130 and 140 GeV at the end of 1995 and at the $e^+e^- \to W^+W^-$ threshold of 161 GeV in 1996. Studies are performed on fermion pair production and the energy evolution of QCD observables. From the measured W pair cross section at 161 GeV, a value for the mass of the W is obtained. The new energy regime in e^+e^- collision is also exploited to extend searches for particles predicted by Supersymmetry and other extensions of the Standard Model.

1 Introduction

The Large Electron-Positron Collider (LEP) at CERN in Geneva has been operated since 1989 at center-of-mass (cms) energies close to the mass of the Z. This first phase (LEP I) has been concluded in 1995. Each of the four experiments, ALEPH, DELPHI, L3, and OPAL, has collected approximately four million Z decays allowing very precise tests of the Standard Model (SM) of electroweak interactions and the determination of many of its parameters. Significant contributions are made to Quantum Chromodynamics, b-quark and tau physics, as well as the search for new particles and phenomena. In particular, the SM Higgs boson is ruled out in the entire mass range from $0 - -65$ GeV by the LEP experiments.

In preparation of the second phase (LEP II), marked by running at energies above the W pair production cross section, LEP was operated at cms energies between 130 and 140 GeV in November 1995 (LEP 1.5). This has been possible after installation of additional super-conducting (SC) radio frequency cavities required by the higher energy loss due to synchrotron radiation at higher beam energies. A total luminosity of about 6 pb^{-1} was delivered by LEP to each of the four experiments. Besides serving as a pilot run for the machine and the experiments to get accustomed to the very different running conditions as compared to the Z this run also provided interesting physics results, in particular, the search for Supersymmetry, which are discussed below.

In 1996 after installation of more cavities, LEP ran at a cms energy of 161 GeV. The main merit of this run is the determination of the W mass from the measured cross section $\mathrm{e^+e^-} \to \mathrm{W^+W^-}$ at the threshold. Also, new kinematic regions in the search for new particles are explored. Preliminary results from about one-third of the data collected at this energy were available at the time of the conference and are included here.

2 Status of LEP

The energy upgrade of the LEP machine requires most importantly the increase of the accelerating power which is achieved by addition of SC cavities. The average energy loss per turn of the circulating particles increases from about 130 MeV at the Z pole to 1 900 MeV for a beam energy $E_\mathrm{b} = 90$ GeV. By October 1995, in total 64 SC cavities were installed increasing the maximum beam energy to

$E_b = 70$ GeV. During the winter shutdown, 80 more units were installed allowing for beam energies above 80 GeV and hence crossing the W pair threshold. In October 1996, a total number of 172 SC cavities will have been installed, which will increase the operational energy to $E_b = 86$ GeV. The successful operation of the machine so far demonstrated the reliable performance of the SC cavity system at its design gradient of 6 MV/m (Refs.[??]).

The performance of the LEP machine is illustrated in Fig. **??**, which shows the delivered integrated luminosity as a function of time from June to August 1996. The setup of the machine was done at the Z pole which provided calibration data for the experiments. In the last week of running at $\sqrt{s} = 161$ GeV, average daily luminosities of 0.6 pb^{-1} were provided to each of the four experiments.

The installation of more cavities is foreseen such that in 1998 the beam energy can be raised to 96 GeV. The goal is to provide an integrated luminosity of 500 pb^{-1} above the W pair threshold to each of the four experiments by the year 2000.

3 Total Cross Sections and Forward-Backward Asymmetries

The LEP experiments study fermion pair production at the new cms energies far above the Z pole. Total cross section measurements are performed for the four reactions

$$\mathrm{e^+e^-} \to \text{hadrons}, \quad \mathrm{e^+e^-} \to \mathrm{e^+e^-}, \quad \mathrm{e^+e^-} \to \mu^+\mu^-, \quad \mathrm{e^+e^-} \to \tau^+\tau^- \ . \qquad (1)$$

In the leptonic final states, the forward-backward asymmetry, A_{FB}, is determined as well.

Cross sections at LEP 1.5 and at LEP II are about two orders of magnitude smaller than at the Z pole. Figure **??** shows the cross section $\mathrm{e^+e^-} \to \mathrm{q\bar{q}}$ as function of the cms energy. The approximate energy range of current and previous $\mathrm{e^+e^-}$colliders is also indicated. The luminosity of $5 - -6$ pb^{-1} collected at $130 - -140$ GeV corresponds to about 1 600 hadron events per experiment. Approximately the same number of events has been observed in 11 pb^{-1} at 161 GeV.

3.1 Radiative Return to the Z

$\sqrt{s}$	140 GeV	161 GeV
$e^+e^- \to$ hadrons	80%	70%
$e^+e^- \to \mu^+\mu^-$	65%	50%

Table 1: Fraction of events with effective cms energies $\sqrt{s'} < 110$ GeV for hadron and muon final states at two cms energies.

At cms energies above the Z pole, initial state radiation (ISR) plays an important role. Radiation of photon(s) by the incoming electrons removes energy from the annihilation process and the fermion production takes place at a lower effective cms energy, $\sqrt{s'}$, where the cross section is different. In particular, if the remaining energy in the e^+e^- system is close to the mass of the Z, m_Z, the annihilation cross section is very high. Consequently, this provides a major contribution to the total cross section $e^+e^- \to f\bar{f}$ and it is called "Radiative Return to the Z." The importance of the return to the Z is illustrated in Fig. **??** which shows the distribution of the effective cms energy of the final-state quark pair in $e^+e^- \to q\bar{q}$ as obtained from a Monte Carlo (MC) calculation for $\sqrt{s} = 161$ GeV. Besides the usual peak at the nominal cms energy with a smooth tail towards lower energies from the radiation of soft photons, one observes that the majority of the events is actually produced at $\sqrt{s'} \approx m_Z$.

Table **??** gives the fraction of events with the fermion pair produced at lower energy ($\sqrt{s'} < 110$ GeV) calculated with the JETSET**?** and KORALZ**?** programs. The relative contribution of events radiated back to the Z becomes smaller with increasing cms energy as the required energy for the ISR photon is higher. In the hadron sample, the fraction of events produced at $\sqrt{s'} \approx m_Z$ is higher than in the muon and tau samples because the ratio of hadron to charged lepton production at the Z is higher than above the Z as the Z couples stronger to quarks than to charged leptons. For the process $e^+e^- \to e^+e^-$ the t-channel boson exchange is dominant above the Z pole. Hence, the resonant s-channel production at the Z is less important for this process (see below).

Because of the different nature of events produced at, or close to, the nominal cms energy and those stemming from decays of real Z bosons, the LEP experiments measure two sets of cross sections and forward-backward asymmetries: for the total sample and the high energy events separated by a cut in the reconstructed

$\sqrt{s'}$ value. The definition of high-energy events differs among the experiments.

3.2 Determination of $\sqrt{s'}$

The effective cms energy is reconstructed assuming a three-body final state, i.e., only one ISR photon (Fig. ??). Then $\sqrt{s'}$ is given by the photon energy E_γ:

$$s' = s - 2E_\gamma\sqrt{s} \; . \tag{2}$$

If the ISR photon is detected, its measured energy can be used to obtain $\sqrt{s'}$. However, in general, photons are emitted at small angles by the incoming electron or positron, and thus often escape detection through the beam pipe. In this case, the photon energy can be determined from the polar angles of the outgoing fermions, Θ_1 and Θ_2 (Fig. ??):

$$E_\gamma = \sqrt{s}\,\frac{|\sin(\Theta_1+\Theta_2)|}{\sin\Theta_1+\sin\Theta_2+|\sin(\Theta_1+\Theta_2)|} \; . \tag{3}$$

Higher order effects like multiple photon emission are taken into account by correcting the cross section and $A_{\rm FB}$ measurements with factors obtained from MC studies. Hadron events are forced into two jets and the quark directions are approximated by the jet axes. A kinematic fit taking into account direction and energy measurements improves the resolution on E_γ and thus $\sqrt{s'}$.

An event $e^+e^- \to$ hadrons $+ \gamma$ recorded with the DELPHI detector at $\sqrt{s} =$ 130 GeV is shown in Fig. ??. In this example, the ISR photon is emitted at a relatively large angle and observed in the forward calorimeter of the detector.

The effective cms energy, reconstructed as described above by L3, for the four final states of Eq. ?? is shown in Fig. ??. The data correspond to a luminosity of 4.3 pb^{-1} at $\sqrt{s} = 161$ GeV. High-energy events are clearly separated from the ones produced with $\sqrt{s'} \approx m_{\rm Z}$. The shapes of the observed distributions are well-described by MC simulations. As mentioned above, the radiative return to the Z is much less pronounced in the e^+e^- final state because the cross section is dominated by t-channel boson exchange.

3.3 Results on Total Cross Sections

The measurements of cross sections at LEP 1.5 are described in Refs..[?,?,?,?] Most of the luminosity was taken at cms energies of 130 and 136 GeV and only a little

amount at 140 GeV. A total number of about 1 600 hadron events has been recorded by each experiment. Recent preliminary results from the 161 GeV run are presented in Ref..[?]

The results of the hadronic cross-section measurements above the Z pole are shown in Fig. ?? for both the total event sample and the high-energy events alone. For the sake of comparison, the results of the four experiments are scaled to the common definition $\sqrt{s'} > 110$ GeV for the high-energy sample.[?] The measurements are compared to the SM expectations as calculated with the program ZFITTER 4.9 (Ref.[?]), and they are found to be in good agreement.

Measurements of leptonic cross sections above the Z pole are shown in Fig. ??. Here the results for $e^+e^- \to \mu^+\mu^-$and $e^+e^- \to \tau^+\tau^-$ are averaged over the four experiments after being adjusted to a common $\sqrt{s'}$ cut. For comparison also, the high-precision measurements at cms energies close to m_Z are displayed. For both reactions, the total cross sections as well as the cross sections for the inclusive high-energy samples are in good agreement with the SM prediction.

3.4 Results on Forward-Backward Asymmetries

The forward-backward asymmetry is defined as

$$A_{FB} = \frac{N_F - N_B}{N_F + N_B}, \tag{4}$$

where N_F and N_B are the number of events in the forward and backward hemispheres. Above the Z, a large fraction of the events is produced with a large acollinearity angle. This creates an ambiguity in the definition of the asymmetry because both final state leptons are often scattered into the same hemisphere. Forward and backward events are defined either by the hemisphere of the negative lepton or by calculating the polar angle in the $\ell^+\ell^-$ rest frame. Different definitions of A_{FB} used by the experiments make it difficult to compare experimental results, especially for the asymmetry of the total sample which includes the radiative return to the Z.

As an example, experimental results from OPAL from the Z pole up to recent measurements based on about 3 pb^{-1} at 161 GeV are shown in Fig. ?? and compared to the SM expectations. Figure 9(a) shows the asymmetry in e^+e^- as function of the cms energy for electron scattering angles $|\cos\Theta_{e^-}| < 0.7$. For most of the energy range, t-channel boson exchange dominates and leads to a

large positive forward-backward asymmetry. The effect of resonant Z production at $\sqrt{s} = m_{\mathrm{Z}}$, where the asymmetry is small, is clearly visible.

The reactions $\mathrm{e^+e^-} \to \mu^+\mu^-$ and $\mathrm{e^+e^-} \to \tau^+\tau^-$ which are expected to have similar asymmetries are combined in Fig. ??(b). The SM expectation for the total sample is shown as a solid line and for the high energy events $\sqrt{s'/s} > 0.8$ as dotted line; the latter is close to the Born-level asymmetry without radiative corrections (broken line). Radiative corrections are huge above the Z pole since the total sample is a mixture of events from high energy with large asymmetry and events at the Z where the asymmetry is small. The observed polar angle distributions for the three lepton species at 161 GeV are shown in Figs. ??(c)–9(e). All measurements are in good agreement with the theoretical expectations.

The measurements at the highest $\mathrm{e^+e^-}$ energies can be compared to results obtained by experiments at lower energies. Figure ?? shows a compilation of forward-backward asymmetry measurements in $\mathrm{e^+e^-} \to \mu^+\mu^-$ performed at $\mathrm{e^+e^-}$ colliders operating below the Z resonance (see Ref.[?] and references therein) together with L3 measurements at and above the Z. Measurements in the gap between the TRISTAN cms energy and m_{Z} are performed using events collected at $\sqrt{s} = m_{\mathrm{Z}}$ which are radiated down to lower energies.[?] Good agreement between the measurements and the SM prediction is observed over the entire energy range up to $\sqrt{s} = 161$ GeV.

4 Determination of the γZ Interference

The total $\mathrm{e^+e^-} \to \mathrm{f\bar{f}}$ cross section, σ_{tot}, is composed of three terms

$$\sigma_{\mathrm{tot}} = \sigma_\gamma + \sigma_{\mathrm{Z}} + \sigma_{\mathrm{int}} \tag{5}$$

describing the contributions of the photon and Z exchange and their interference, σ_{int}. While running at the Z pole, the LEP experiments mainly measured the Z contribution whereas the other two represented small corrections preventing their precise measurement. In particular, the γZ interference contributes significantly only below and above the Z pole. This can be seen from Fig. ?? which shows the relative contribution of σ_{int} to the total hadronic cross section. Above the Z pole, most of the sensitivity is contained in the part of the cross section at high effective cms energy.

	$J_{\rm had}$
LEP $\sqrt{s} \approx m_{\rm Z}$	$+0.18 \pm 0.34$
incl. $130 - 140$ GeV	-0.21 ± 0.20
incl. TOPAZ	-0.07 ± 0.16
Standard Model	$+0.22$

Table 2: LEP results on the hadronic interference term $J_{\rm had}$ from fits in the S-matrix framework using different data sets. The last line shows the SM expectation.

In lowest order, the contribution of the γZ interference can be written as

$$\begin{aligned} \sigma_{\rm int} &= \frac{4\pi\alpha^2}{3} J_{\rm f} \frac{s - m_{\rm Z}^2}{(s-m_{\rm Z}^2)^2 + s^2\Gamma_{\rm Z}^2/m_{\rm Z}^2} \\ J_{\rm f} &= \frac{G_{\rm F}\, m_{\rm Z}^2}{\sqrt{2}\,\pi\,\alpha} q_{\rm e} q_{\rm f}\, g_{\rm V}^{\rm e} g_{\rm V}^{\rm f} \end{aligned} \tag{6}$$

with $\Gamma_{\rm Z}$ denoting the total width of the Z, α the QED, and $G_{\rm F}$ the Fermi coupling constants. The interference term $J_{\rm f}$ is proportional to the product of the charge, $q_{\rm f}$, and the vector coupling constants $g_{\rm V}^{\rm f}$ of the fermions involved.

Of special interest is the hadronic interference term defined as the sum over the five quark flavors produced at LEP energies

$$J_{\rm had} = \sum_{\rm u,d,c,s,b} J_{\rm q}\,. \tag{7}$$

About 90% of the Z decays recorded by the LEP experiments are hadronic final states which therefore dominate the results on parameters like the mass and total width of the Z. When determining Z parameters from a Breit-Wigner fit to the measured cross sections at the Z resonance, the hadronic interference term usually is set to its SM expectation. This way, the quark couplings, and hence, the flavor composition of hadronic Z decays, are prescribed to their SM expectations. This introduces some model dependence into the determination of Z parameters.

Alternatively, the hadronic interference term can be measured by treating it as a free parameter in the fit. For instance, this is done is the S-matrix approach.**?** In Table **??**, the results on $J_{\rm had}$ averaging over the four LEP experiments are shown with and without using the data collected at LEP 1.5. One notices that the few hundred hadron events at high energy collected per experiment significantly

	m_{Z} [MeV]
LEP $\sqrt{s} \approx m_{\mathrm{Z}}$	$91\,189.3 \pm 6.2$
incl. $130 - 140$ GeV	$91\,193.6 \pm 4.0$
J_{had} fixed to SM	$91\,191.3 \pm 2.0$

Table 3: LEP results on the Z mass obtained in the S-matrix framework with and without including measurements at $130 - -140$ GeV and compared to the result obtained with a fixed hadronic interference term.[?]

improve the precision on J_{had} as compared to the Z data alone. Further improvement is achieved when including the measurement of the hadron cross section at $\sqrt{s} = 57.8$ GeV performed by the TOPAZ Collaboration.[?] The measurements of J_{had} agree reasonably well with the SM expectation.

At the Z pole, the γZ interference contribution changes its sign. Varying the hadronic interference term would therefore change the position of the peak while leaving the width and height of the resonance curve unchanged. Figure ?? shows the correlation of m_{Z} and J_{had} as obtained from a fit to LEP data in the S-matrix framework.[?] Both 68% contours, with and without including LEP 1.5 data, are shown. The improvement on J_{had} translates hence to a reduction of the error on m_{Z} determined this way which depends less on the validity of the SM (Table ??). For comparison, the combined LEP Z mass obtained with a J_{had} fixed to its SM value is quoted as well.[?]

5 Studies of QCD in $e^+e^- \rightarrow$ hadrons

The hadron events recorded during the runs at $130 \leq \sqrt{s} \leq 161$ GeV are used to perform studies on the energy evolution of observables and to compare them to the predictions based on QCD. For these studies, events radiated to lower effective cms energies are excluded. Details on the QCD tests performed with the data collected at $130 \leq \sqrt{s} \leq 140$ GeV can be found in Refs..[?,?,?,?] Some examples of these studies are presented here.

A first example is the measurement of the average charged particle multiplicity in hadronic events, $< n_{ch} >$. The DELPHI experiment, using their hadron sample

with $\sqrt{s'} > 122$ GeV, finds for $\sqrt{s} = 130$ GeV (Ref.[?])

$$< n_{ch} > = 23.84 \pm 0.91 \pm 0.52, \tag{8}$$

where the first error is statistical and the second systematic.

In Fig. **??**, this result is compared to measurements at lower cms energies. The evolution of the average charged particle multiplicity is well-described by QCD including next-to-leading log corrections up to the new measurement when using $\alpha_s(130 \text{ GeV}) = 0.105$.

In addition to counting charged particles from quark fragmentation, their momentum spectrum is studied at the new cms energies. From the particle momentum, p, normalized to the beam energy, one defines the quantity

$$\xi_{\mathrm{p}} = -\ln x_{\mathrm{p}} \qquad \text{with } x_{\mathrm{p}} = \frac{p}{E_{\mathrm{b}}} \tag{9}$$

emphasizing such the low-energy part of the spectrum. The distribution obtained by OPAL from the first part of their 161 GeV data is shown at the top of Fig. **??**. The observed spectrum is compared to the PYTHIA[?] MC program and to a QCD fit in next-to-leading log approximation. From the fit, the position of the maximum, ξ_0, is obtained which can be calculated in QCD. At the bottom of Fig. **??**, measurements of ξ_0 at different energies are compared to the QCD calculation. Again, the new measurements are in good agreement with the expected energy evolution up to $\sqrt{s} = 161$ GeV.

The LEP experiments determine the average thrust in $\mathrm{e^+e^-} \to$ hadrons events at the new energies. The ALEPH result is compared to measurements at $\sqrt{s} = m_{\mathrm{Z}}$ and other experiments at lower energies in Fig. **??**. These data are compared to several MC models predicting the narrowing of jets at higher energies. The measurement at 133 GeV is in agreement with the expectation.

All QCD observables investigated at high energies are consistent with their expected energy evolution using the α_{s} value measured by the LEP experiments at the Z pole. Hence, the new measurements can be used to extract α_{s} at higher energy. Table **??** summarizes the results on α_{s} obtained from various event shape variables at the average LEP 1.5 energy of $\sqrt{s} = 133$ GeV. As expected, these α_{s} values are smaller than $\alpha_{\mathrm{s}}(m_{\mathrm{Z}})$ but the statistical errors are still large. Detailed investigations of error correlations on the experimental and theoretical side should allow us to confirm the running of α_{s} from the Z up to the new cms energies.

	$\alpha_s(133\ \mathrm{GeV})$
ALEPH	0.119 ± 0.008
DELPHI	0.119 ± 0.008
L3	0.107 ± 0.008
OPAL	0.110 ± 0.010

Table 4: Measurements of α_s at $\sqrt{s} = 133$ GeV using hadronic event shape variables.[?,?,?,?]

Measurements of the strong coupling constant α_s at different momentum transfer Q are compared in Fig. **??**. The experimental results are in agreement with the expected running of α_s.

,clip

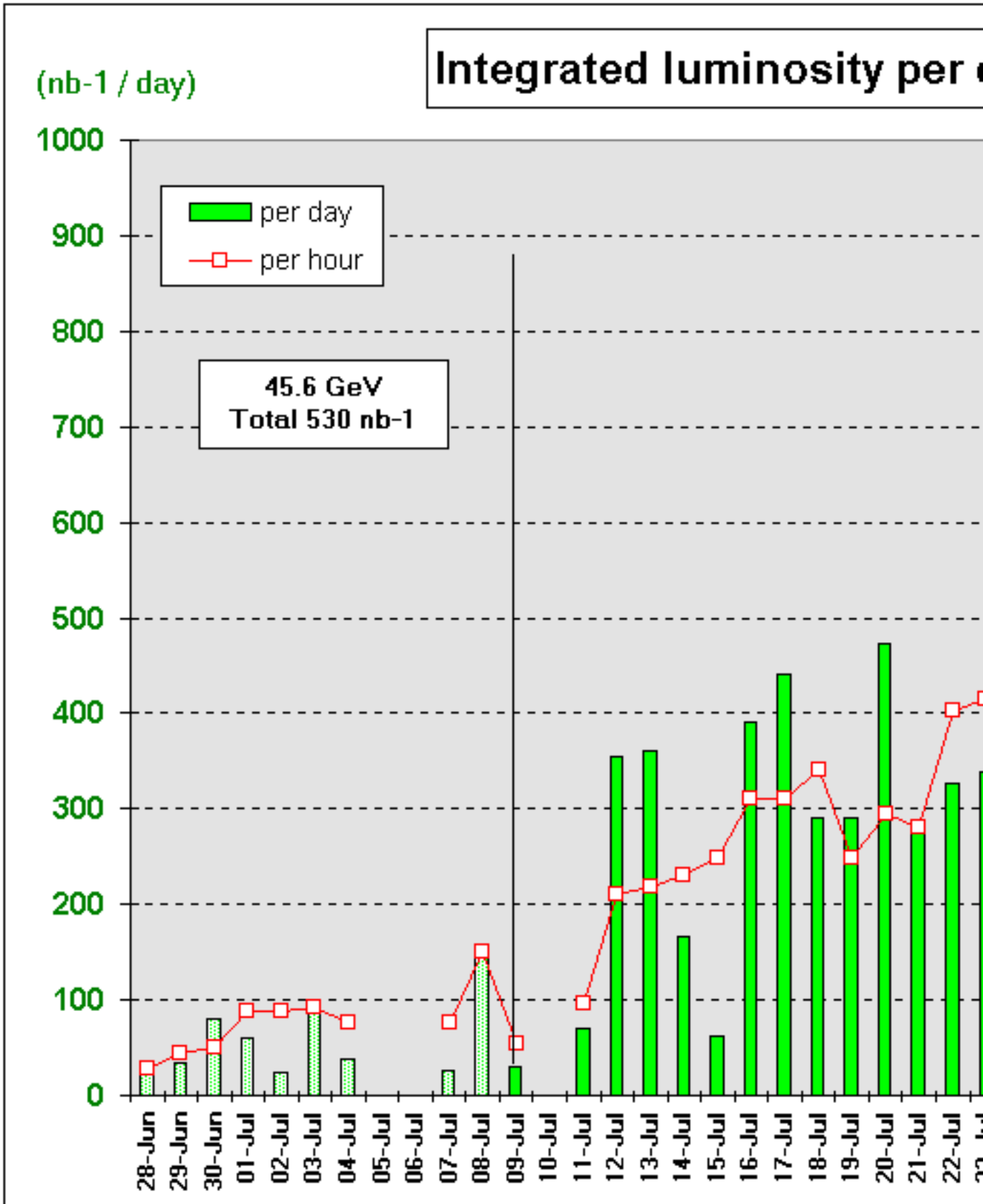
Integrated luminosity per
(nb-1 / day)
1000
900
800
700
600
500
400
300
200
100
0
per day
per hour
45.6 GeV
Total 530 nb-1
28-Jun
29-Jun
30-Jun
01-Jul
02-Jul
03-Jul
04-Jul
05-Jul
06-Jul
07-Jul
08-Jul
09-Jul
10-Jul
11-Jul
12-Jul
13-Jul
14-Jul
15-Jul
16-Jul
17-Jul
18-Jul
19-Jul
20-Jul
21-Jul
22-Jul

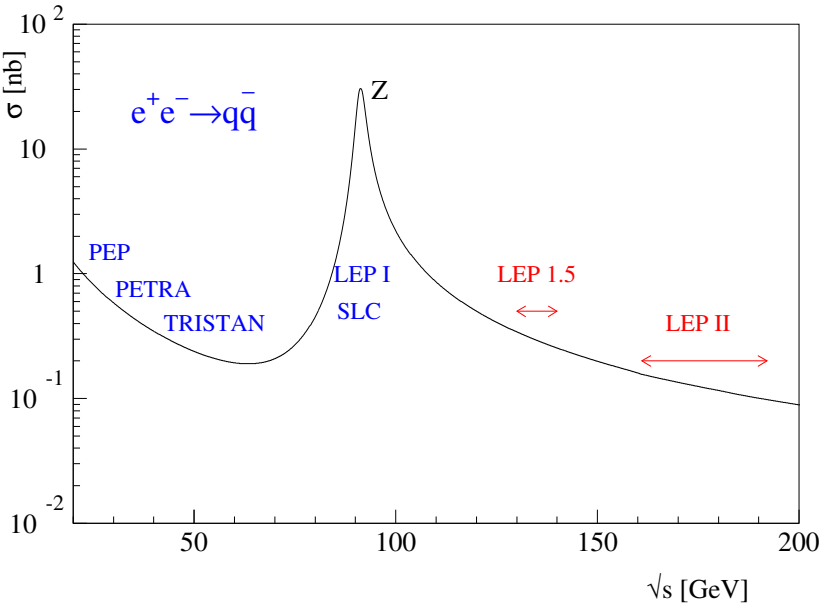

Figure 2: The cross section $e^+e^- \to q\bar{q}$ as function of the cms energy. The approximate energy ranges of previous and current e^+e^- colliders are indicated.

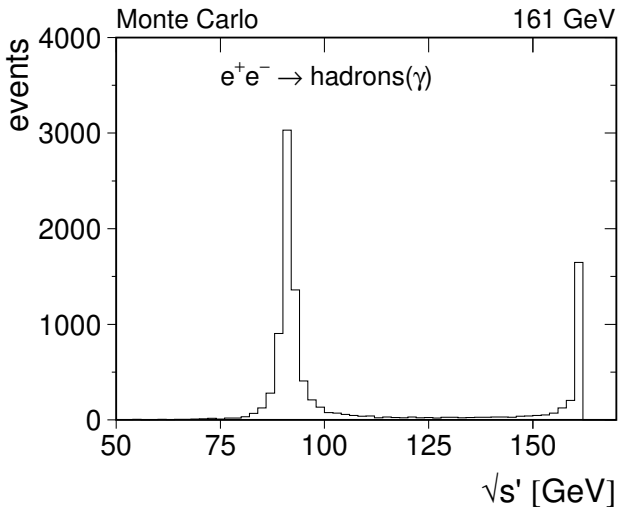

Figure 3: Distribution of the effective cms, $\sqrt{s'}$, in the reaction $e^+e^- \to$ hadrons obtained from MC calculation at $\sqrt{s} = 161$ GeV.

,clip

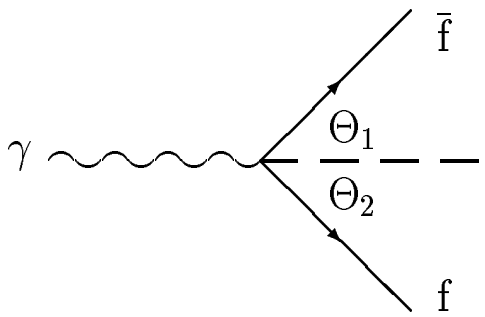

Figure 4: Reconstruction of the photon energy from the polar angles of the outgoing fermion-antifermion pair.

,clip

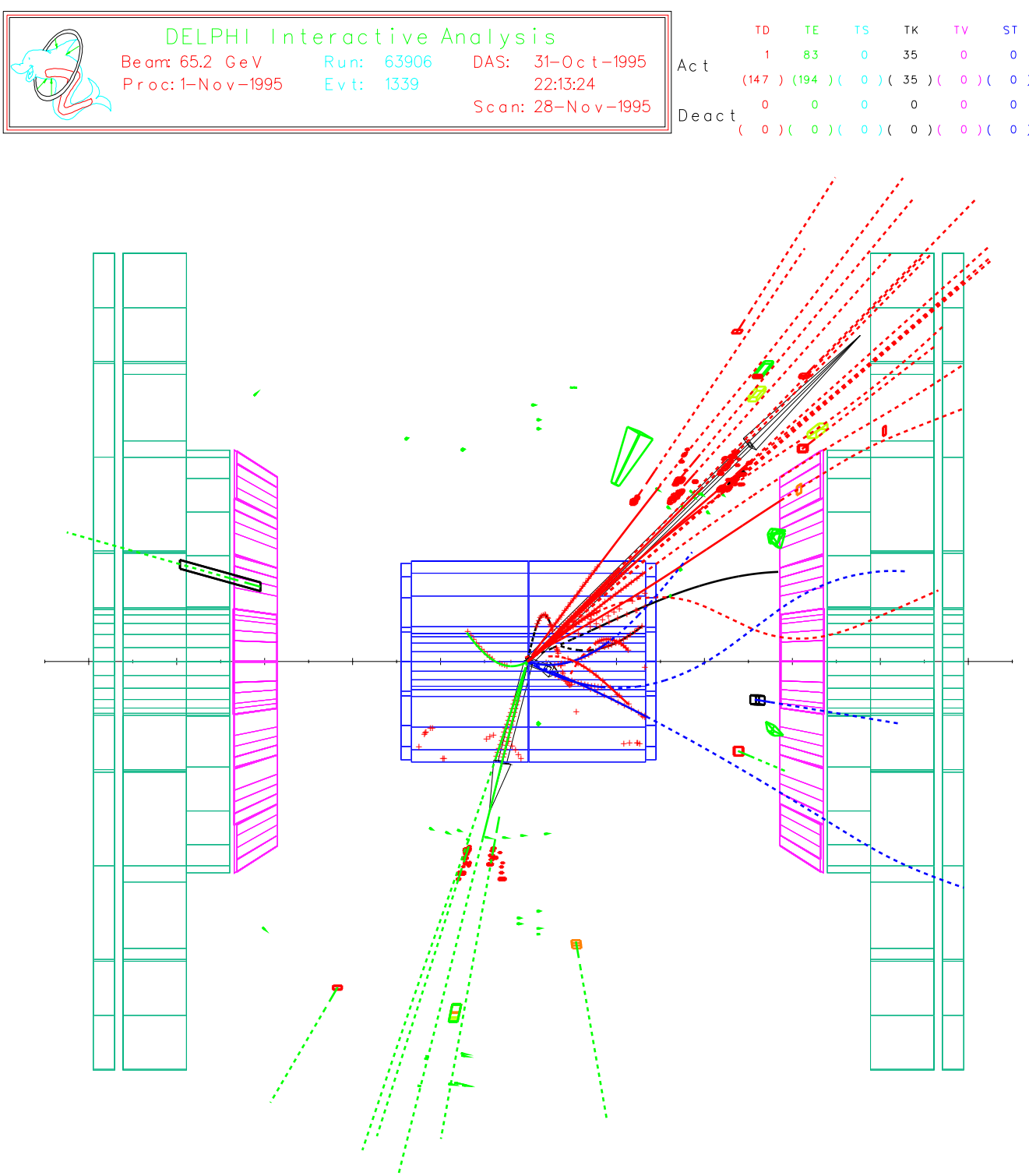

Figure 5: Example of an event $e^+e^- \to$ hadrons $+\gamma$ in the DELPHI detector (side view). Here the initial state photon is observed in the left forward region of the detector.

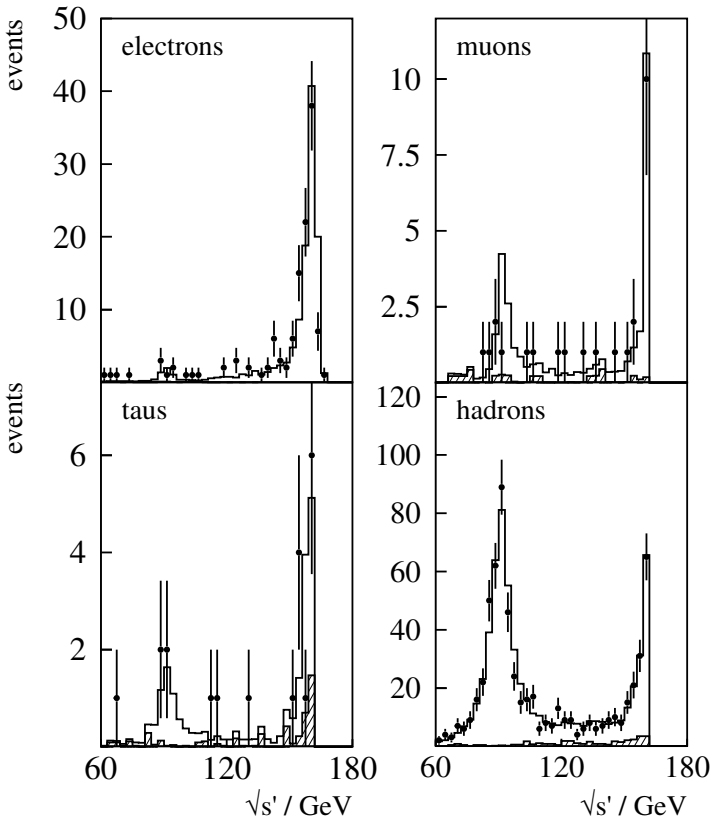

Figure 6: Distributions of the reconstructed effective cms energy $\sqrt{s'}$ for the four reactions of Eq. ?? obtained at $\sqrt{s} = 161$ GeV by L3. The points with error bars represent the data. Signal and background MC expectations are shown as open and hatched histograms, respectively.

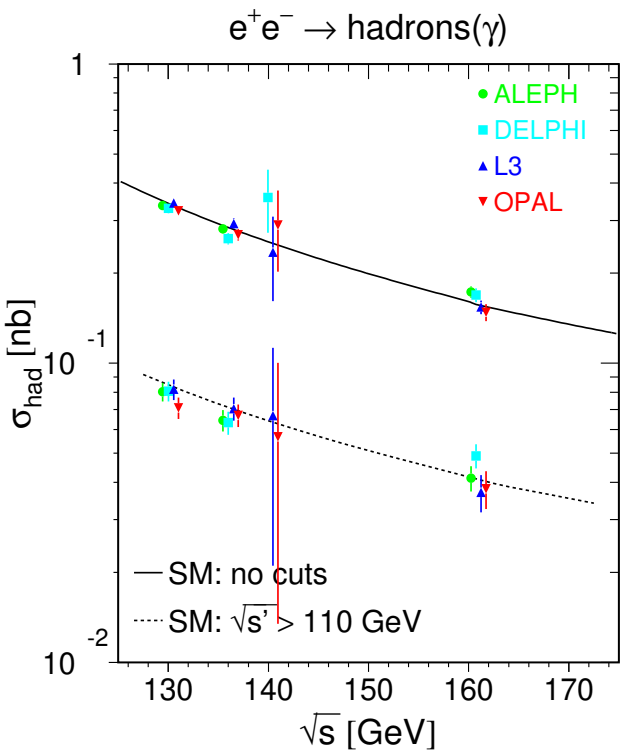

Figure 7: Cross section $e^+e^- \to$ hadrons measured by the LEP experiments between 130 and 161 GeV. The total cross section as well as the cross section at high $\sqrt{s'}$ are shown and compared to the SM expectation (solid and broken line, respectively).

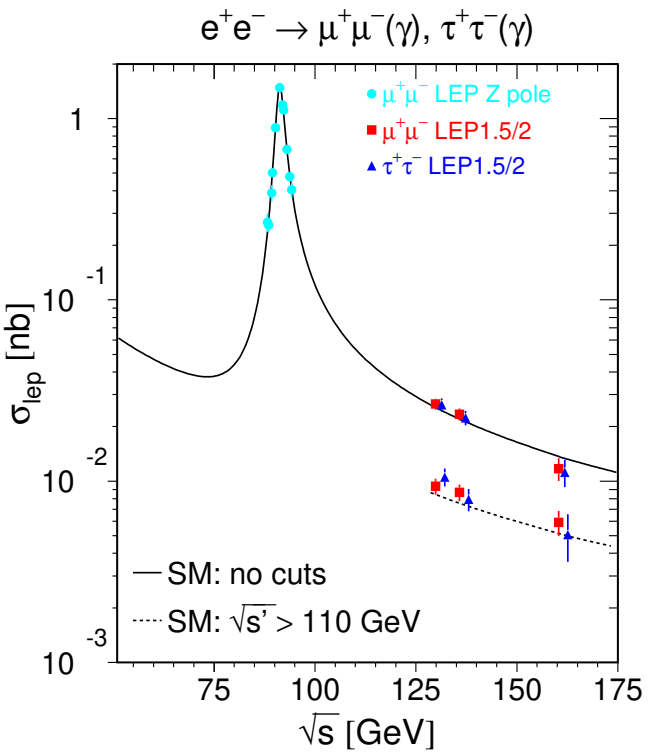

Figure 8: Cross sections $e^+e^- \to \mu^+\mu^-$ and $e^+e^- \to \tau^+\tau^-$ averaged over the four LEP experiments at function of $\sqrt{s}$ from the Z pole to 161 GeV. The total cross sections as well as the cross sections for high $\sqrt{s'}$ are shown and compared to the SM expectation (solid and broken line, respectively).

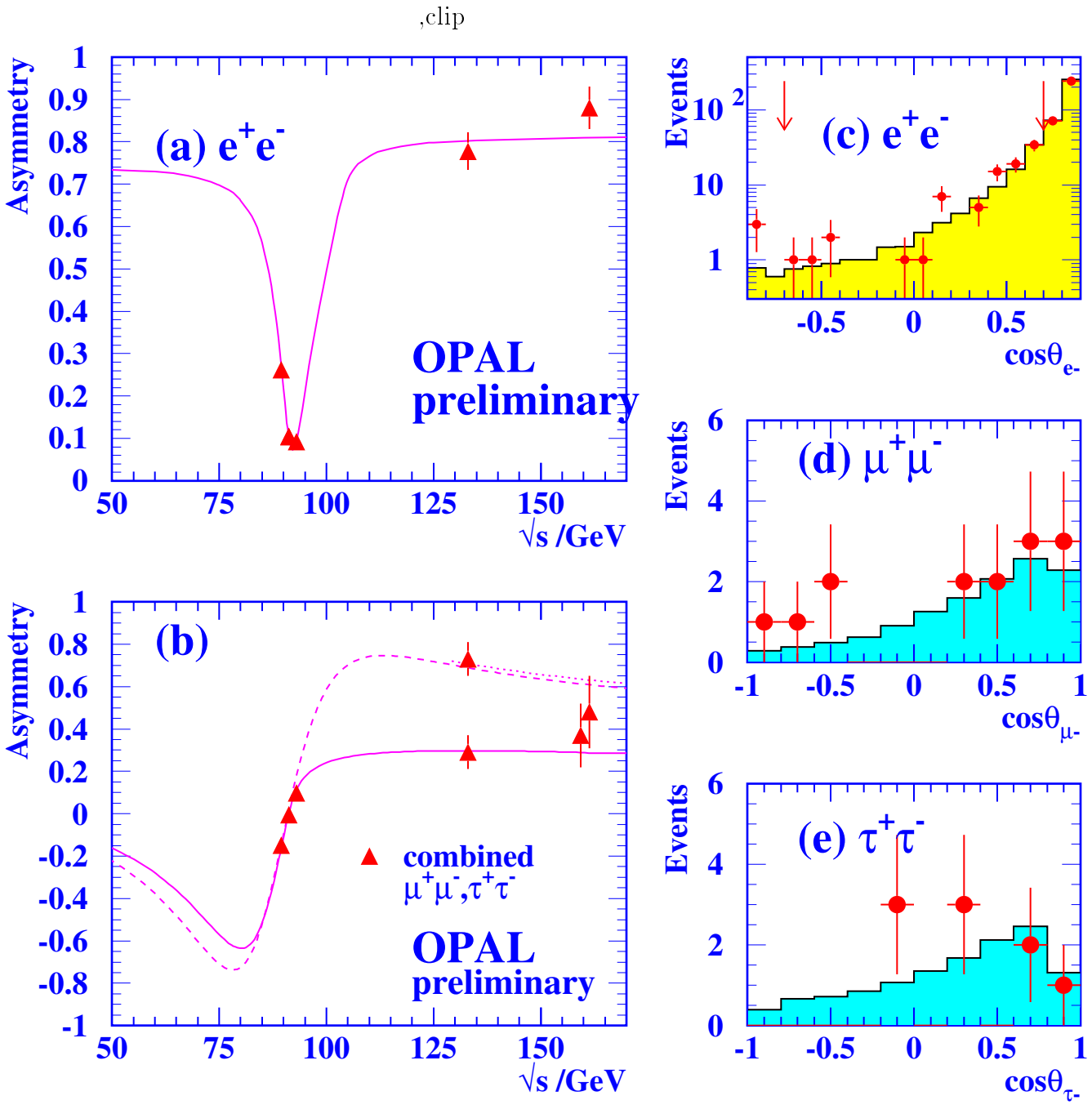

Figure 9: Measured e^+e^- forward-backward asymmetry (a) for $|\cos\Theta_{e^-}| < 0.7$ as a function of the cms energy as obtained by OPAL. (b) shows the combined muon and tau asymmetry as a function of energy for the total and the high-energy samples ($\sqrt{s'/s} > 0.8$). The SM expectations are represented as solid lines for the total, and dotted line for the high-energy sample. The broken line shows the Born-level asymmetry. The polar angle distributions at 161 GeV of the negative leptons are shown in plots (c)–(e).

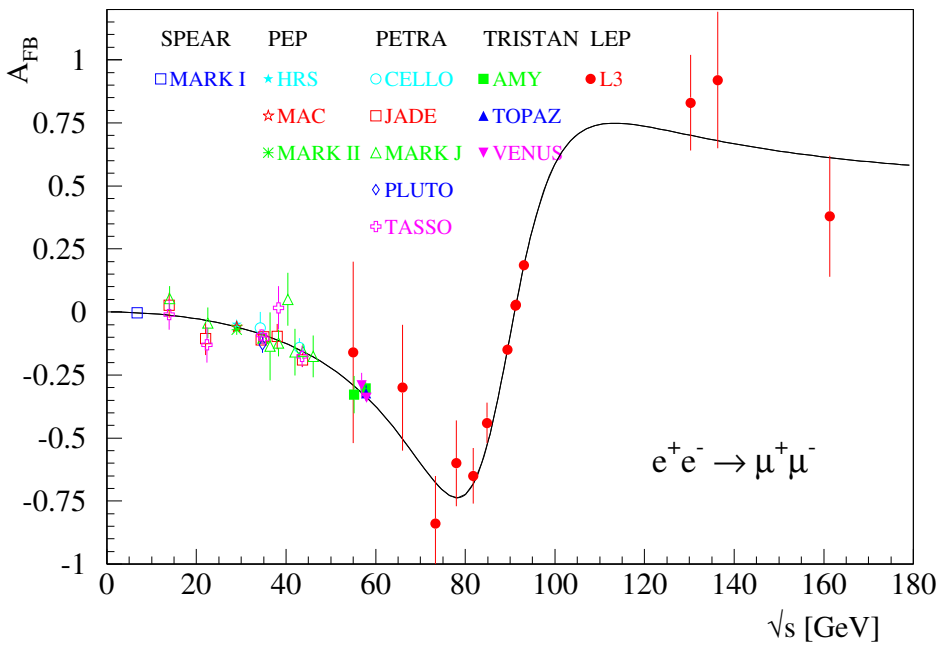

Figure 10: Measurements of the forward-backward asymmetry in $e^+e^- \to \mu^+\mu^-$ as a function of the cms energy performed by experiments at various e^+e^- colliders. The solid line represents the Born-level expectation.

,clip

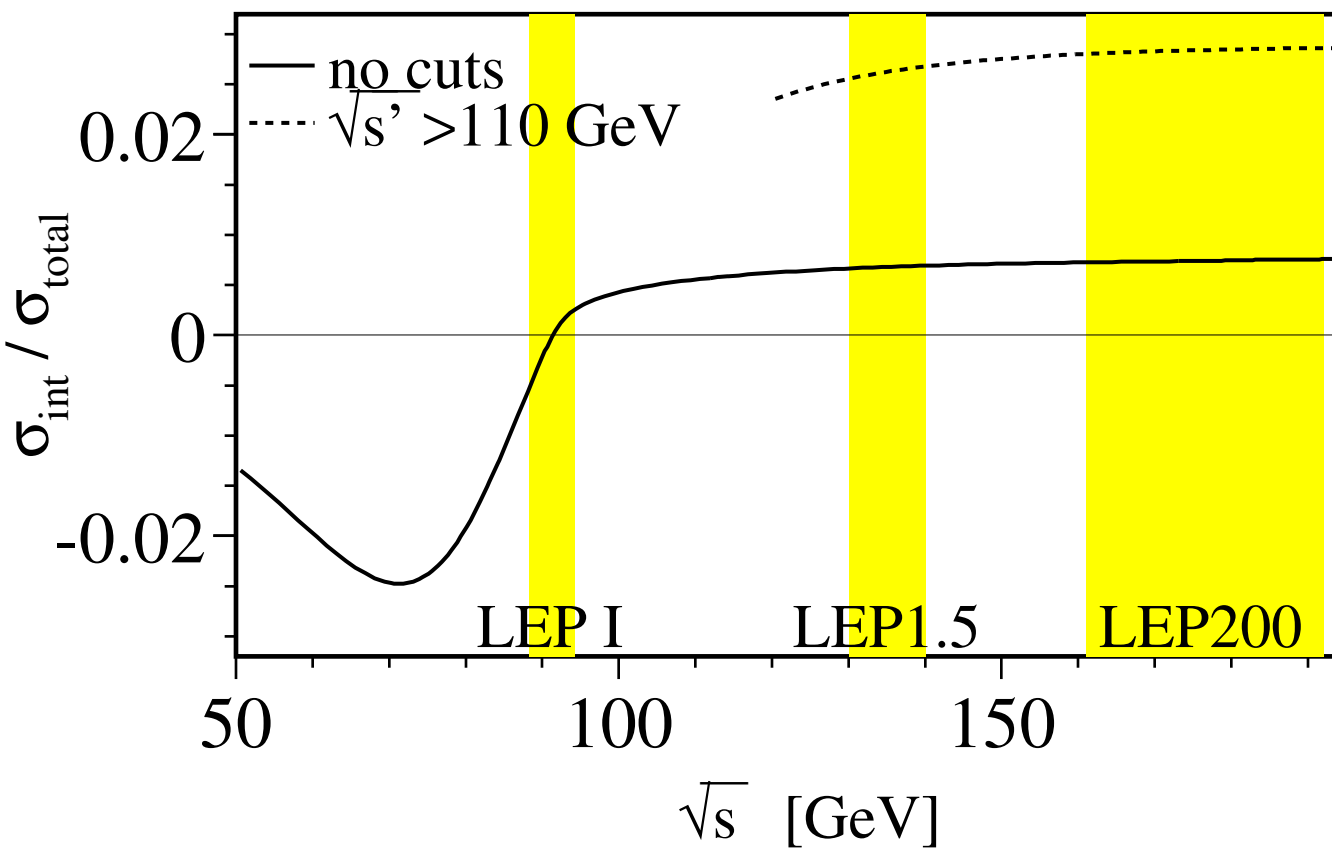

Figure 11: The relative contribution of the γZ interference to the total hadronic cross section as a function of the cms energy. The broken line shows this ratio for the cross section at high effective cms energies.

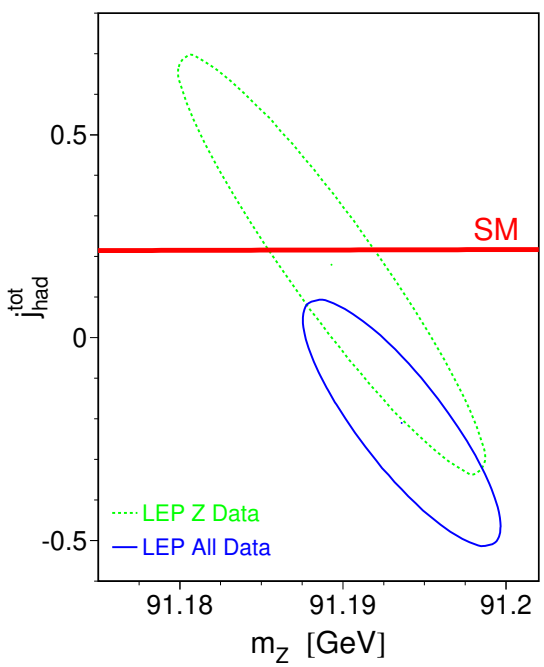

Figure 12: Contours (68% C.L.) in the m_{Z}-J_{had} plane using LEP data at the Z pole only (broken line) as well as including LEP 1.5 results (solid line). The horizontal line shows the SM expectation for J_{had}.

,clip

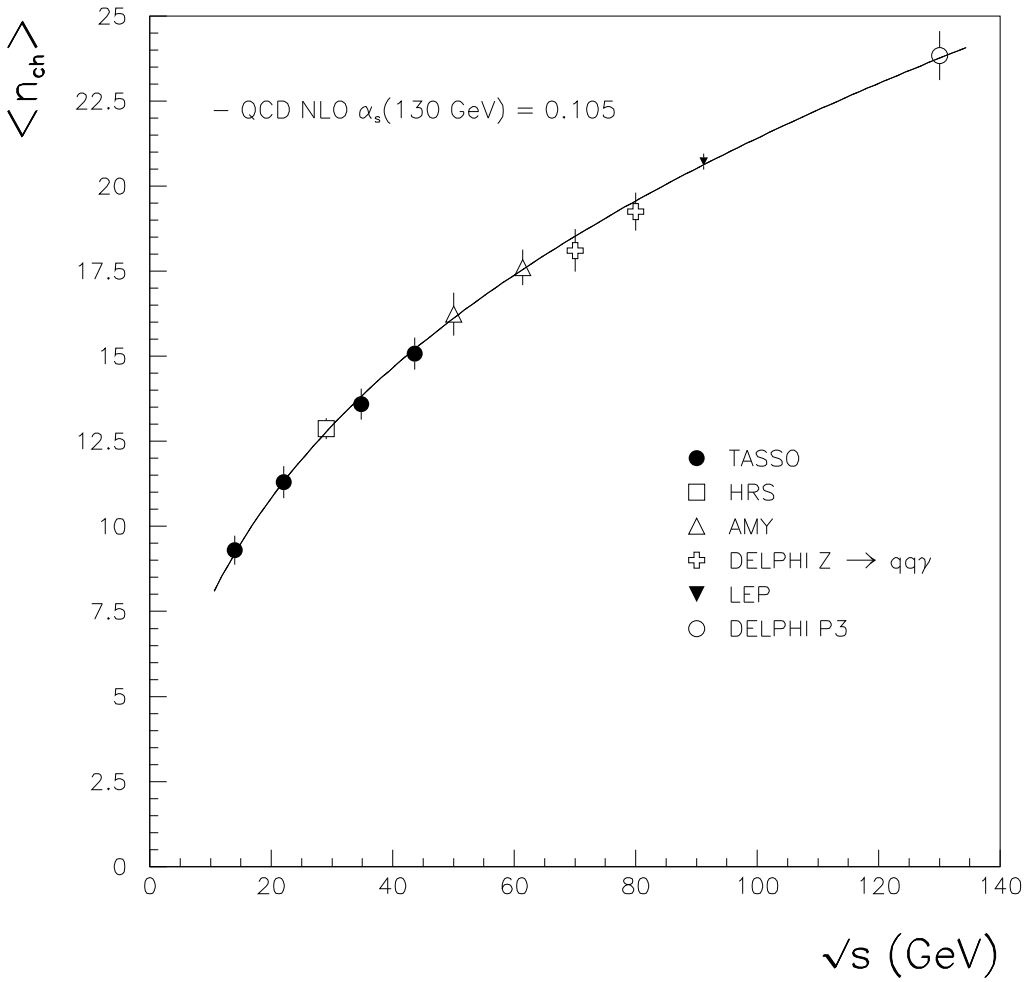

Figure 13: The average charged particle multiplicity in $e^+e^- \to$ hadrons measured by DELPHI at 130 GeV, compared to measurements at lower energies and to the QCD expectation.

Figure 3: Measured multiplicity at 130 GeV, compared with lower energy measurements and with a fit to a prediction from QCD in Next to Leading Order.

,clip

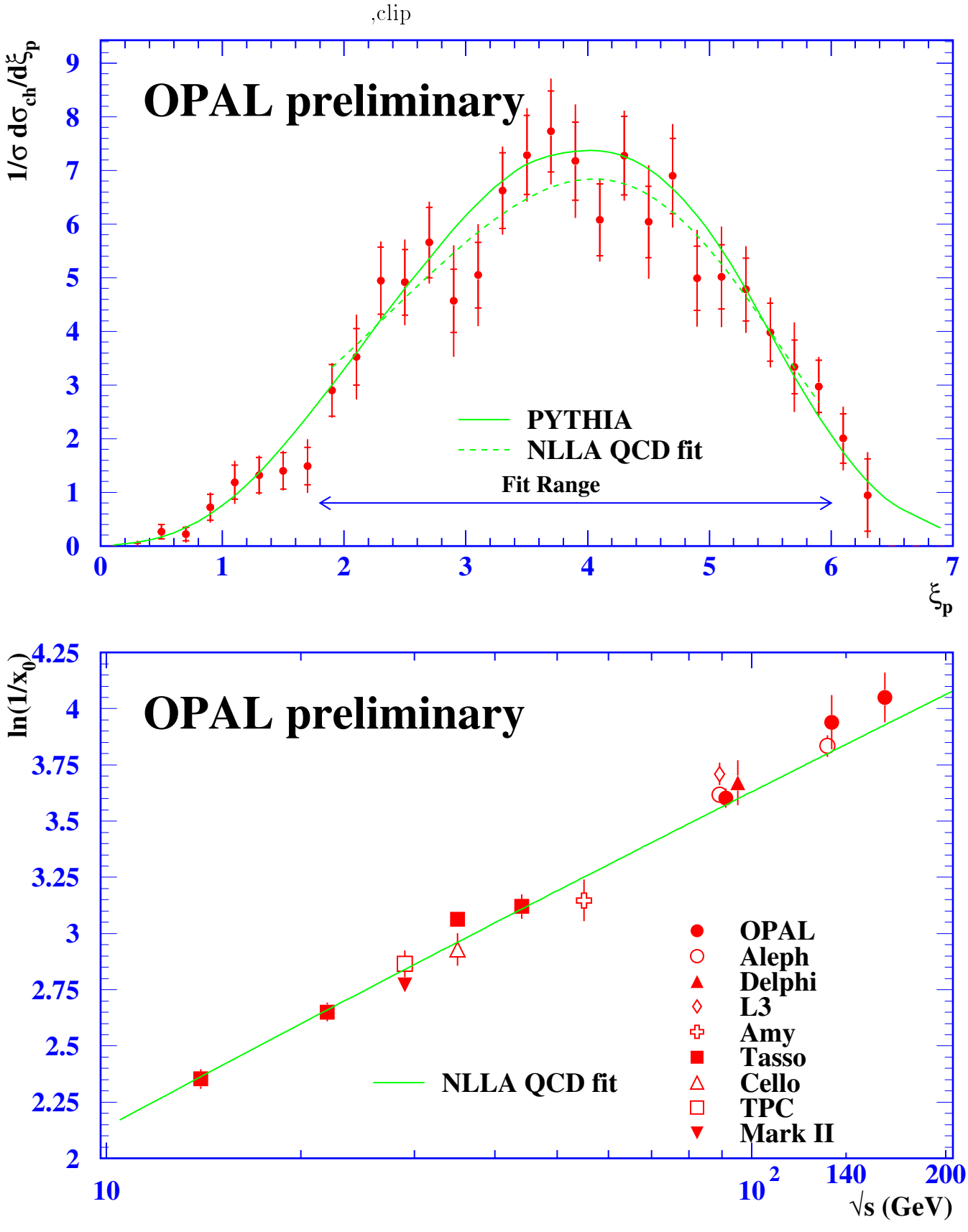

Figure 14: Top: The distribution of ξ_p observed at 161 GeV by OPAL compared to the PYTHIA program and next to leading log QCD calculation

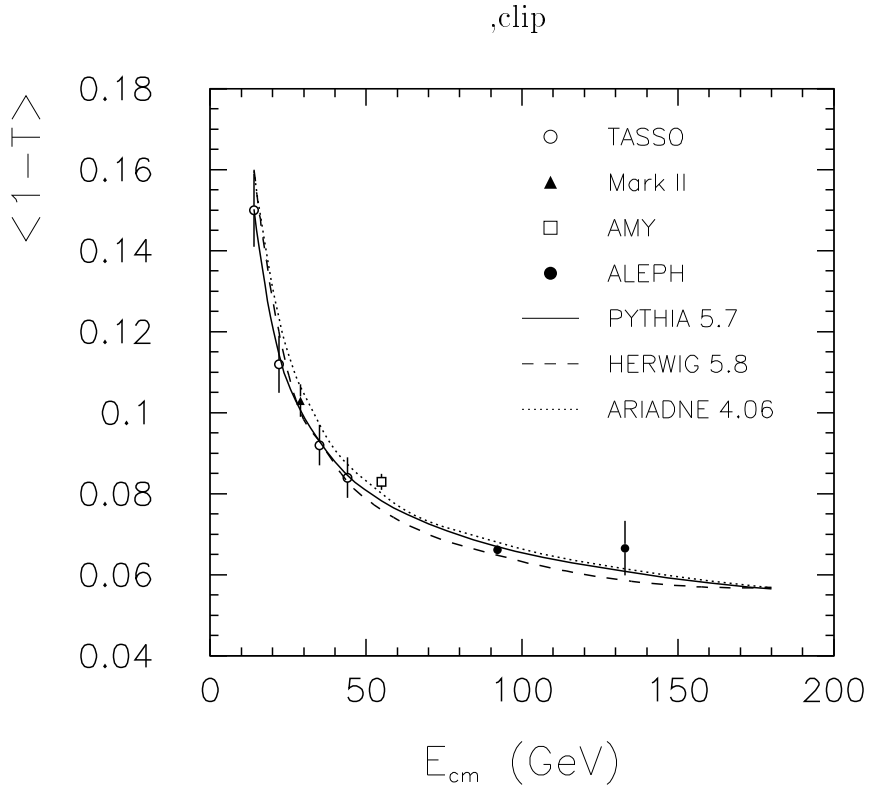

Figure 6: Mean value of $1-T$ versus E_{cm} as measured at various centre-of-mass energies, and the predictions of several Monte Carlo models.

Figure 15: Evolution of the average thrust in $e^+e^- \to$ hadrons events. The ALEPH result at 133 GeV is compared to measurements at lower energies and various MC calculations.

The JETSET $O(\alpha_s^2)$ model is of particular interest for four-jet studies, because it contains the exac $O(\alpha_s^2)$ matrix element for four-parton final states. PYTHIA, on the other hand, uses a parton showe model based on the leading-logarithm approximation, supplemented by a matching of the three-jet rate t the $O(\alpha_s)$ matrix element. A disadvantage of the $O(\alpha_s^2)$ matrix-element model is that the mean particl multiplicity is poorly described when using model parameters tuned at $E_{cm} = 91.2$ GeV (cf. Fig. 3). I order to provide a more realistic test of the jet rates, the two parameters a and b of the Lund symmetri fragmentation function (see [4]) were adjusted from $a = 1.0$ to 1.1 and $b = 0.495\,\mathrm{GeV}^{-2}$ to $0.4\,\mathrm{GeV}^{-}$ resulting in a mean charged particle multiplicity of $N_{ch} = 23.8$ at $E_{cm} = 133$ GeV, in approximat agreement with the data.

Despite the differences between the two models at parton level, the predicted four-jet rates are similar The measured four-jet rate is observed to be lower than predicted at small values of the jet-resolutio parameter y_{cut}, but is greater than predicted for $y_{cut} > 0.01$. A further analysis of four-jet events base on the same data sample will be given in a forthcoming paper [18]. As expected, the matrix elemen model is unable to predict the five-jet rate, because at $O(\alpha_s^2)$ a maximum of four final state partons ca be described.

6 Determination of α_s

,clip

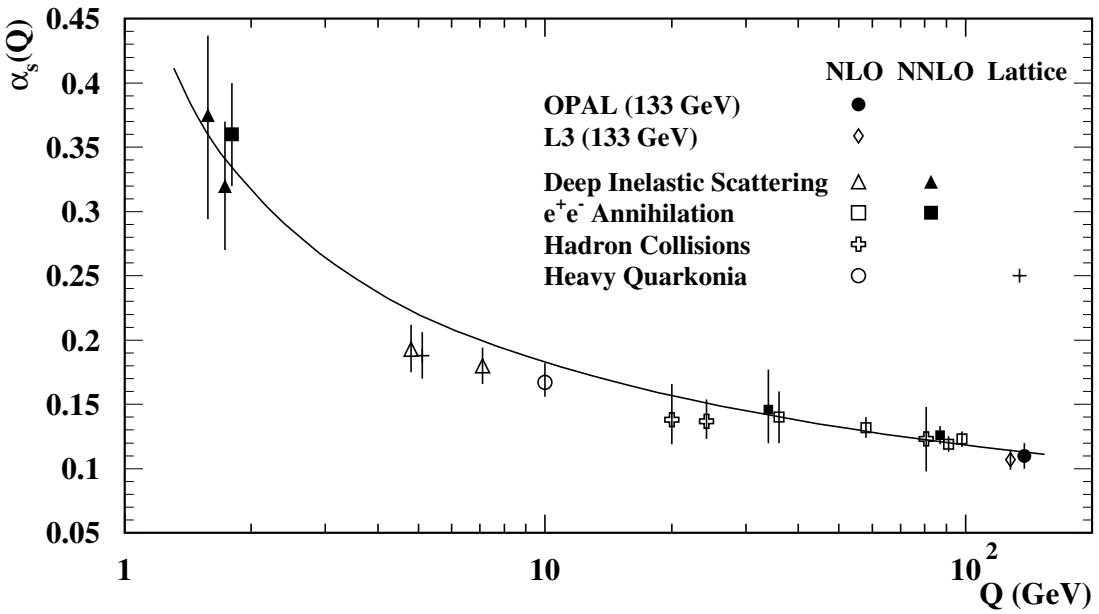

Figure 16: Measurement of the strong coupling constant α_s at different energies. New LEP measurements at $\sqrt{s} = 133$ GeV are compared to measurements at the Z and various other determinations at lower energies. The solid line represents the second order QCD prediction for $\alpha_s(m_Z) = 0.120$(Ref.).

Figure 9: Values of α_s at different energies. The labels NLO and NNLO refer to the order of calculations fitted to extract α_s measurements. NLO corresponds to $\mathcal{O}(\alpha_s^2)$ in e^+e^- annihilations, and NNLO to $\mathcal{O}(\alpha_s^3)$. The label Lattice refers to α_s values determined from lattice QCD calculations. The curve shows the second order QCD prediction for α_s with $\alpha_s(M_{Z^0})$=0.120.

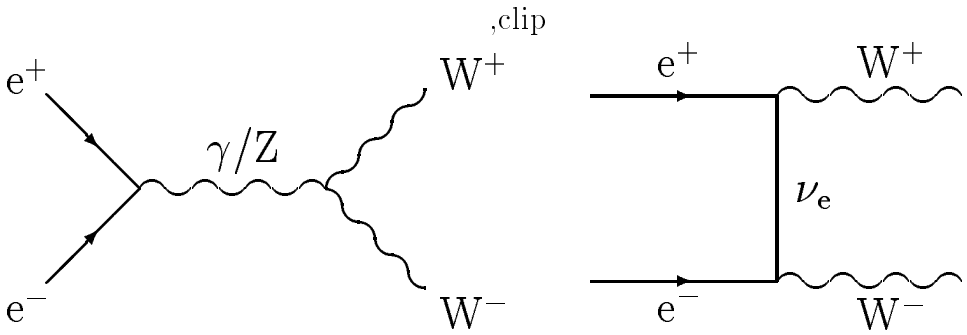

Figure 17: Feynman diagrams contributing to the reaction $e^+e^- \rightarrow W^+W^-$ in lowest order.

6 W Pair Production at LEP

The second phase of the LEP program, marked by the increase of the cms energy above the threshold for the process $e^+e^- \rightarrow W^+W^-$, has started in 1996. This reaction proceeds by the two Feynman diagrams depicted in Fig. **??**: s-channel photon or Z exchange and t-channel electron neutrino exchange. Both individual diagrams diverge at high energies, and only their sum with the couplings predicted by the SM preserves unitarity. Of particular interest are the couplings at the three boson vertex arising from the non-Abelian structure of the SM of electroweak interactions. These will be tested experimentally to the percent level during the next years at LEP II (Ref.**?**).

The first goal is to determine the mass of the W, m_{W}, from the measured cross section at the threshold. Figure **??** shows the cross section as a function of the cms energy around threshold for five different W mass values. These mass values are chosen 200 MeV apart and in the vicinity of the combined measurement from $p\bar{p}$ colliders. The curves are calculated with the program GENTLE,**?** which includes initial state radiative corrections and the finite width of the W. The best separation between the curves and hence the highest sensitivity for m_{W} is achieved for a cms energy of 161 GeV. The point with error bars indicates the statistical precision on m_{W} one experiment would have with 25 pb^{-1} luminosity and an average selection efficiency for W^+W^- final states of 50%.

6.1 Selection of W Pairs

The branching fractions of the W into hadrons and into each of the lepton

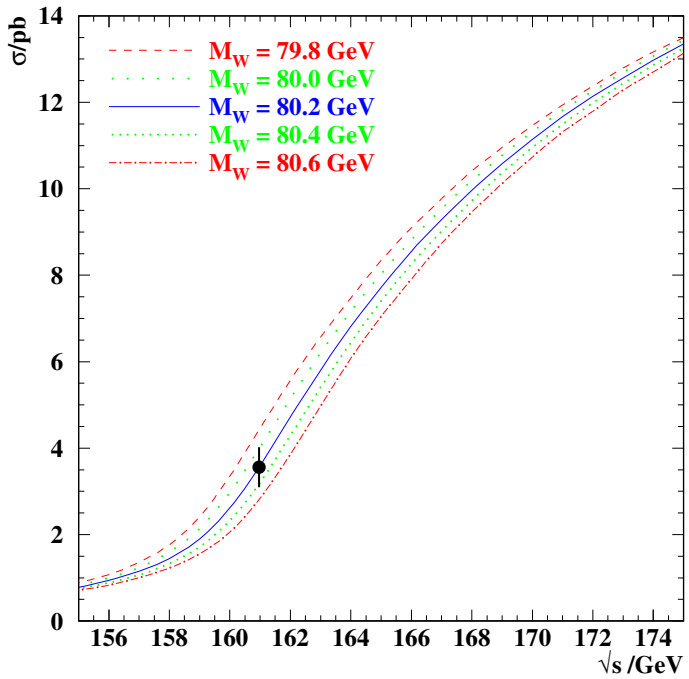

Figure 18: The cross section $e^+e^- \to W^+W^-$ in the threshold region for different W mass values. The point indicates the statistical precision obtainable with an integrated luminosity of 25 pb^{-1} and 50% selection efficiency.

generations has been measured at $p\bar{p}$ colliders to be[?]

$$\begin{aligned} BR(W \to q\bar{q}') &= 67.9 \pm 1.5\% \\ BR(W \to \ell\nu) &= 10.8 \pm 0.4\%, \end{aligned} \tag{10}$$

in agreement with the SM prediction. In the reaction $e^+e^- \to W^+W^-$ one distinguishes three event classes as observed in the detector which are listed in Table **??** with their relative fractions.

Events where both W bosons decay into quarks are selected as four-jet hadron events. To suppress four-jet background from $e^+e^- \to \gamma/Z \to$ hadrons, the jet-pair masses are required to be close to m_W. Usually, kinematic fits are performed to increase the resolution on the jet-pair mass. It should be noted that for $\sqrt{s} =$ 161 GeV, the total hadronic cross section is about 50 times larger than the cross section for W pair production.

The second event class is marked by the presence of two jets with a jet-pair mass of approximately m_W, an energetic charged lepton, and large missing energy due to the neutrino. To keep background from two-fermion production under

,clip

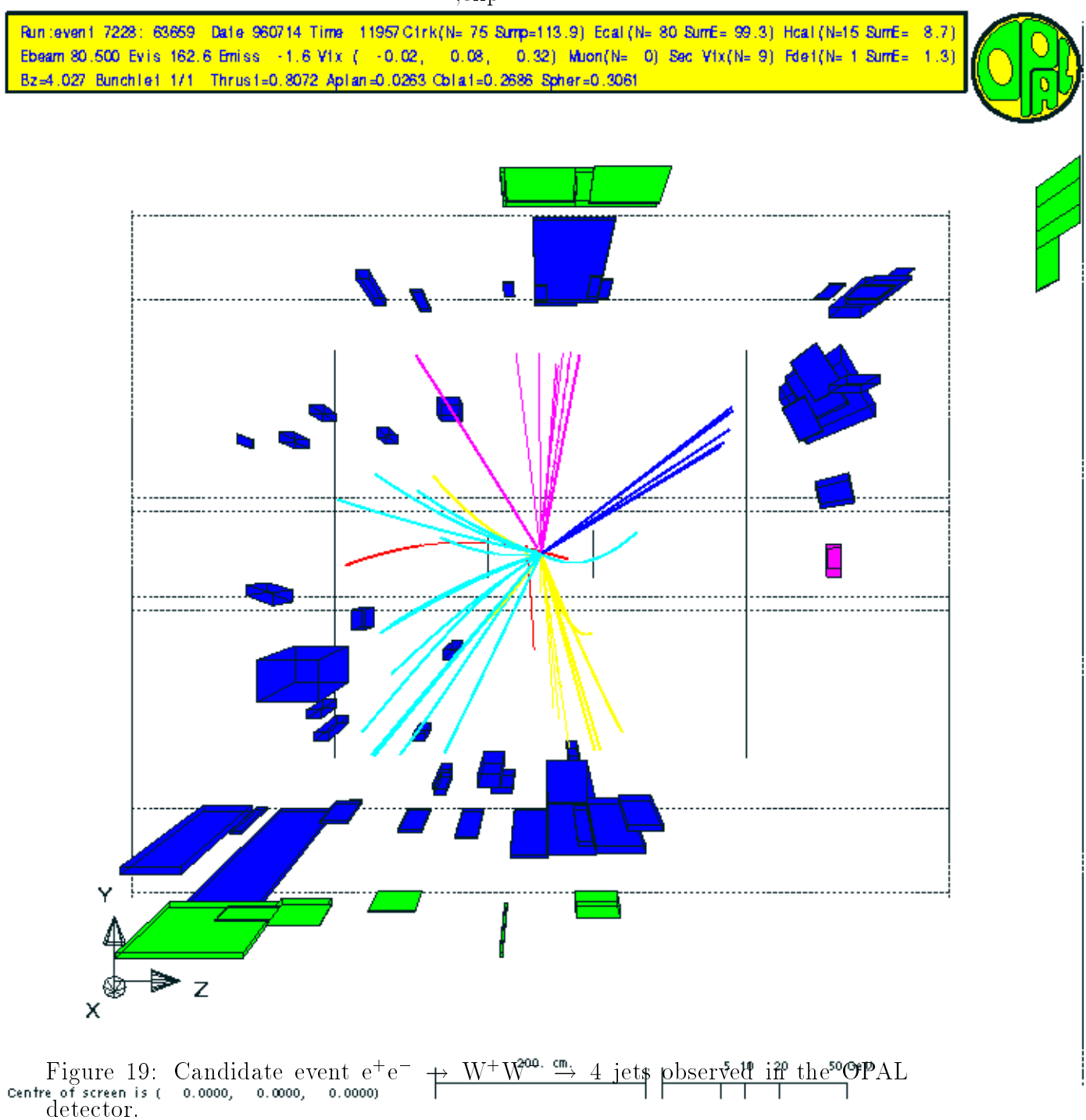

Figure 19: Candidate event $e^+e^- \to W^+W^- \to$ 4 jets observed in the OPAL detector.

	Event class	Fraction
$e^+e^- \to W^+W^-$	$\to$ 4 jets	46%
	$\to \ell\nu + 2$ jets	44%
	$\to \ell\nu + \ell'\nu'$	10%

Table 5: Classes of W pair events as observed in the detectors and their relative abundance ($\ell = e, \mu, \tau$).

Experiment	$\int \mathcal{L}\, dt$ [pb^{-1}]	σ_{WW} [pb]
ALEPH	3	$4.9^{+1.9}_{-1.6}$
DELPHI	5	$3.5^{+1.5}_{-1.3}$
L3	6	$2.9^{+1.3}_{-1.1}$
OPAL	3	$3.9^{+1.8}_{-1.4}$

Table 6: Integrated luminosity analyzed by the time of the conference and results on the $e^+e^- \to W^+W^-$ cross section as obtained by the LEP experiments.

control, events are retained only if the lepton is isolated from the jets. The decay $W^+ \to \tau^+\nu_\tau$ can be identified by the hadronic decay of the τ lepton giving rise to a narrow jet containing one or three charged hadrons.

If both W bosons decay into leptons, two oppositely charged leptons are seen in the detector. The process $e^+e^- \to \ell^+\ell^-$ is suppressed requiring missing energy and the two lepton candidates to be acoplanar.

Figures **??**, **??**, **??**, and **??** show some examples of $e^+e^- \to W^+W^-$ events selected by the LEP Collaborations in the first part of the 1996 run at 161 GeV.

6.2 First Results on $e^+e^- \to W^+W^-$ Cross Section

Preliminary results on the W pair cross section at the threshold obtained by the LEP experiment using the first part of the 1996 data are summarized in Table **??**. The luminosity analyzed so far corresponds to $5 - -10$ events seen by each experiment. These results can be combined to an average value of**?**

$$\sigma_{WW} = 3.6 \pm 0.7 \qquad \text{at } \sqrt{s} = 161.3 \pm 0.2 \text{ GeV}. \tag{11}$$

It should be noted that the total luminosity collected by the four LEP experiments

during the summer of 1996 is about 11 pb^{-1} per experiment, such that very soon more precise measurements of the $\mathrm{e^+e^-} \to \mathrm{W^+W^-}$ cross section at 161 GeV will be available.

6.3 W Mass Determined from Threshold Cross Section

The LEP average on the W pair cross section (Eq. **??**) can be converted into a value of the W mass. This method intrinsically implies the validity of the SM, in particular, the couplings at the three-boson vertex. Figure **??** shows the $\mathrm{e^+e^-} \to \mathrm{W^+W^-}$ cross section as a function of m_W for the average LEP cms energy of $\sqrt{s} = 161.3$ GeV. From the curve, one reads the preliminary LEP result on m_W**?**

$$m_\mathrm{W} = 80.4 \pm 0.3 \pm 0.1(\mathrm{LEP})\ \mathrm{GeV}. \tag{12}$$

The second error represents the current precision on the knowledge of the LEP beam energy as obtained from preliminary magnet calibrations.**?** Both errors are expected to be reduced in near future.

The result presented in Eq. **??** is in good agreement with the measurement of m_W from Fermilab**?** and the mass value that can be inferred from the precise measurements of electroweak radiative corrections at LEP I and SLC:**?**

$$\begin{aligned} m_\mathrm{W} &= 80.37 \pm 0.15\ \mathrm{GeV} \qquad \text{Fermilab} \\ m_\mathrm{W} &= 80.36 \pm 0.05\ \mathrm{GeV} \qquad \text{LEP I \& SLC.} \end{aligned} \tag{13}$$

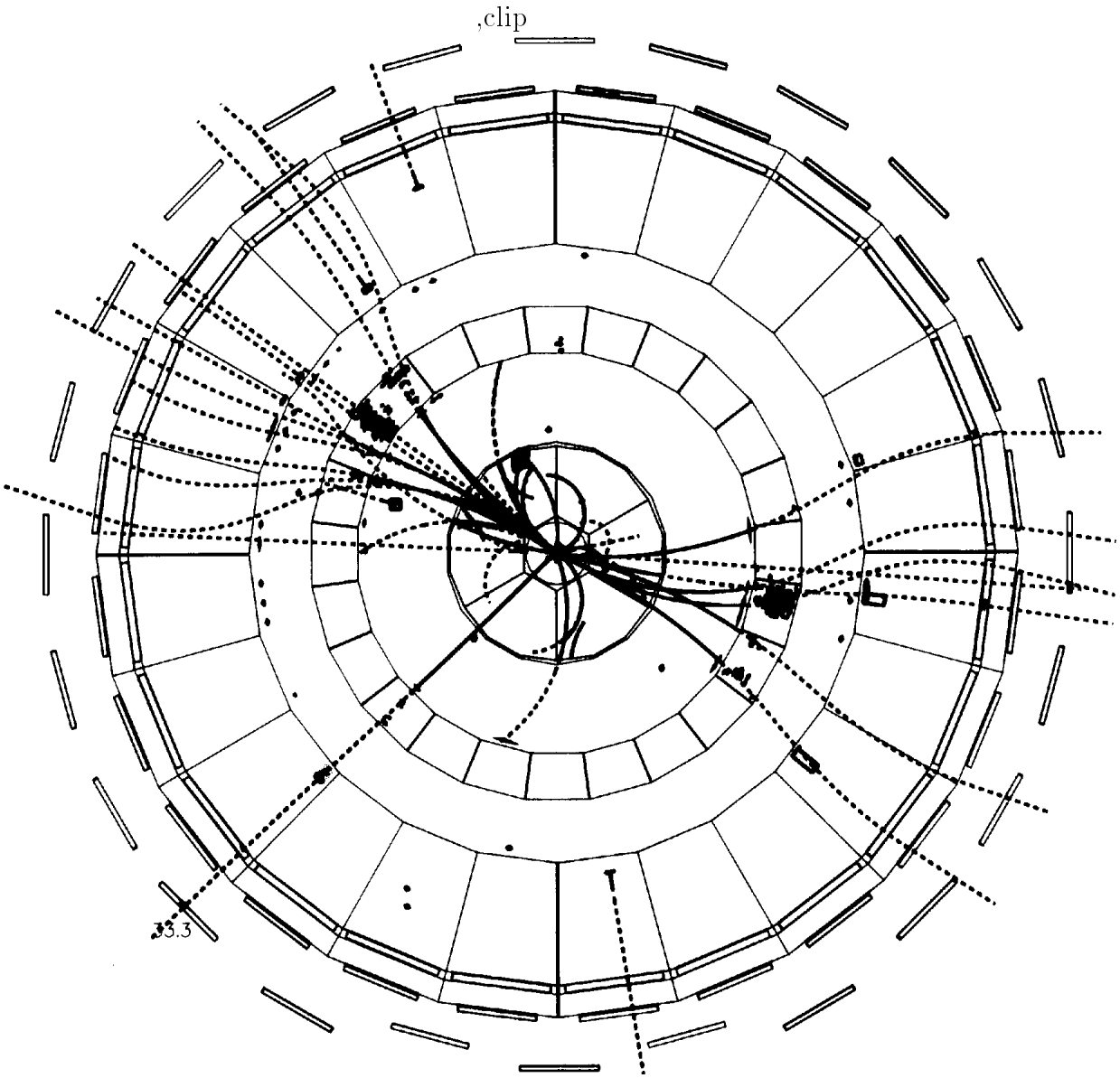

Figure 20: Candidate event $e^+e^- \to W^+W^- \to q\bar{q}'\,\mu^-\bar{\nu}_\mu$ observed in the DELPHI detector. The isolated high momentum track in the lower left part stems from the muon.

y96649MnichNb

Run # 658004 Event # 2394 Total Energy : 142.63 GeV

,clip

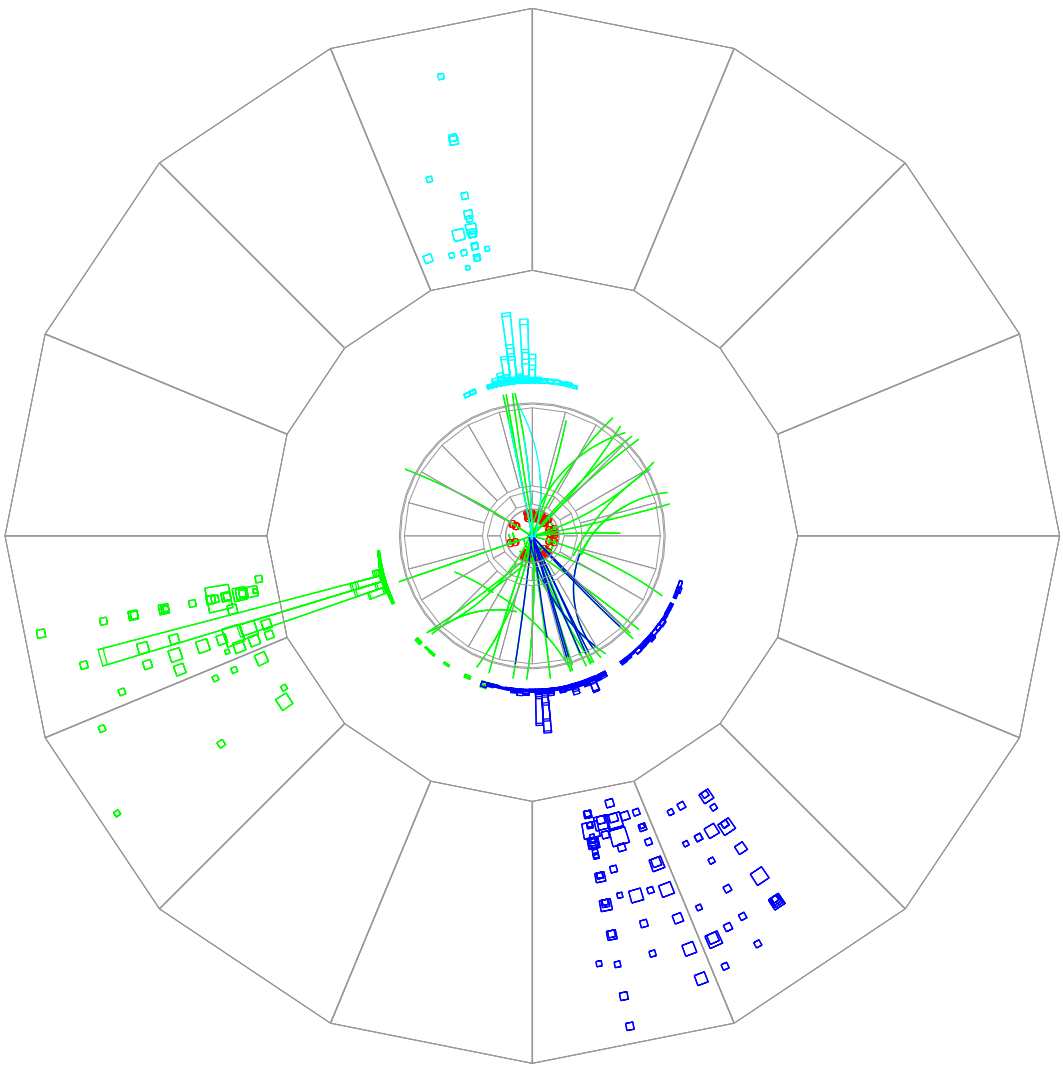

Figure 21: Candidate event $e^+e^- \to W^+W^- \to q\bar{q}'\,\tau^-\bar{\nu}_\mu$ observed in the L3 detector. The narrow jet containing one charged particle on the left side is interpreted as the tau lepton from W decay.

Transverse Imbalance : .3745		**Longitudinal Imbalance :** -.1460
Thrust : .6963	**Major :** .6772	**Minor :** .0916
Event DAQ Time : *960717 61053*		

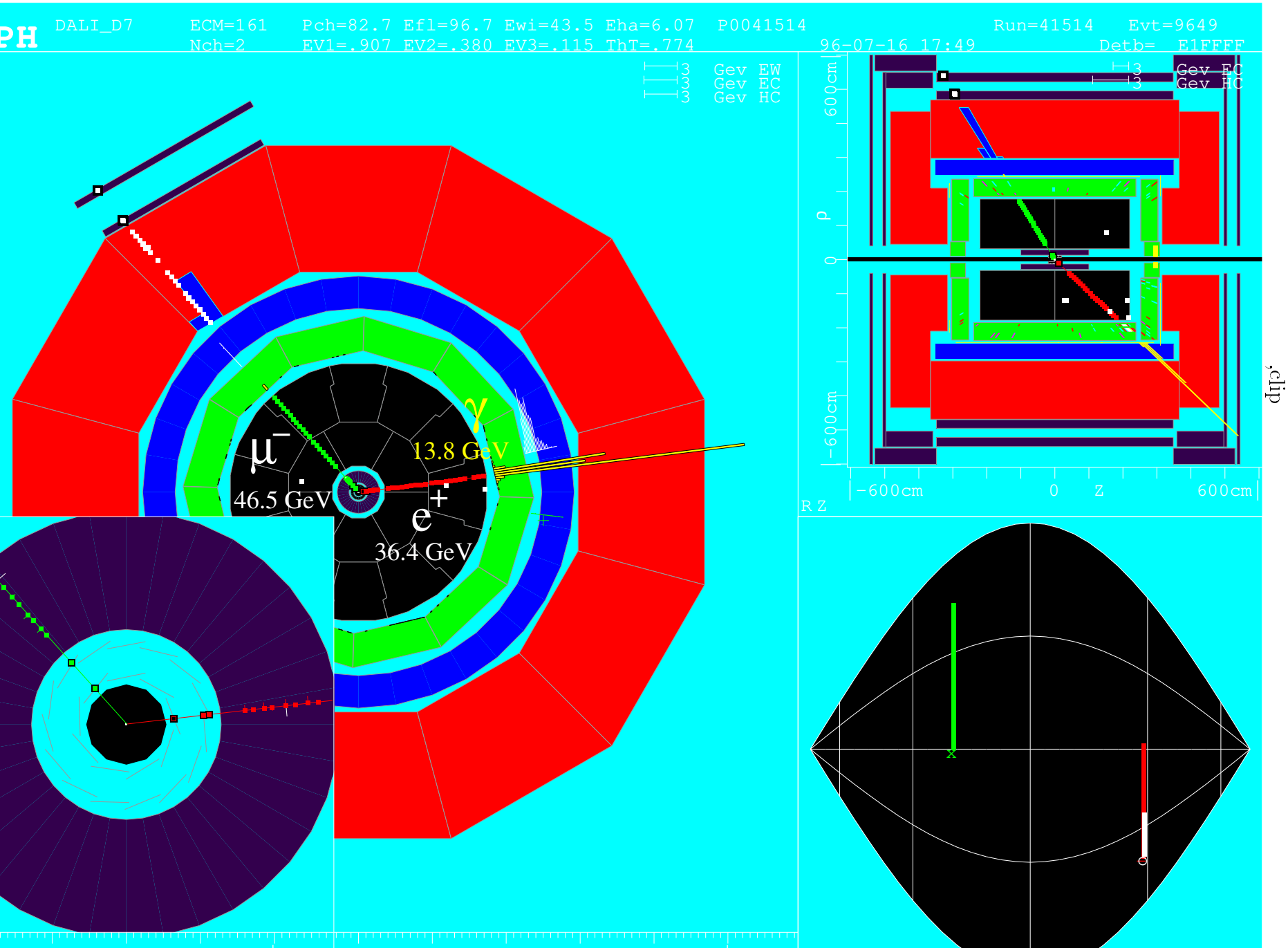
PH
DALI_D7 ECM=161 Pch=82.7 Efl=96.7 Ewi=43.5 Eha=6.07 P0041514
Nch=2 EV1=.907 EV2=.380 EV3=.115 ThT=.774
Run=41514 Evt=9649
96-07-16 17:49
Detb= E1FFFF
3 Gev EW
3 Gev EC
3 Gev HC
μ⁻
46.5 GeV
γ
13.8 GeV
e⁺
36.4 GeV
600cm
0
-600cm
Z
R Z
,clip

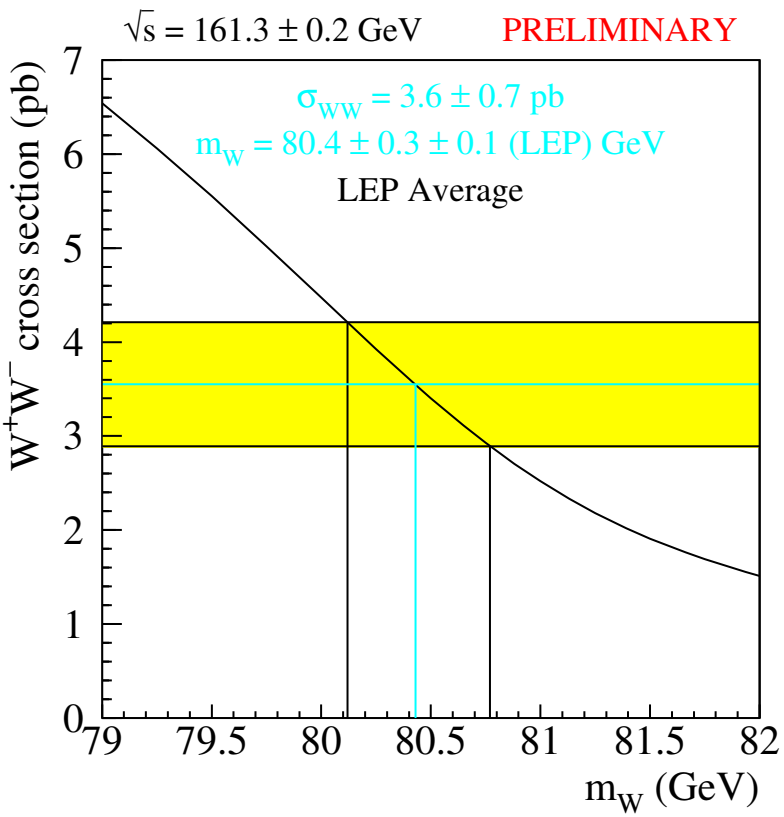

Figure 23: The cross section $e^+e^- \to W^+W^-$ as a function of the W mass for $\sqrt{s} = 161.3$ GeV calculated with GENTLE.[?] The band shows the combined LEP result (Eq. ??) and the derived W mass.

7 Search for Supersymmetry

The search for new particles predicted by Supersymmetry[?] (SUSY) has been carried out by the LEP experiments at the Z resonance. No experimental evidence for SUSY has been found, and limits on particle masses and model parameters are set.[?] For most of the presumed SUSY particles, the kinematic range accessible has been explored at LEP I, and further improvements cannot be expected from more luminosity at $\sqrt{s} = m_Z$ (Ref.[?]).

High cross sections in the order of several picobarn are expected for a wide range of SUSY parameter space in the kinematically accessible region at LEP 1.5 and in the 1996 run at 161 GeV, in particular, for chargino pair production $e^+e^- \rightarrow \tilde{\chi}^+\tilde{\chi}^-$. This very fact was one of the motivations for a short run at $130--140$ GeV at the end of 1995 because already with a modest integrated luminosity of several inverse picobarn, the chargino could be discovered if it existed or else the saturated LEP I limits could be improved.

Here some results on SUSY searches in the framework of the Minimal Supersymmetric Model (MSSM) are presented. Searches for charginos and neutralinos at LEP 1.5 are published in Refs..[?,?,?,?,?,?]

The free parameters of the MSSM are the gaugino mass at the weak scale M_2, the mass scale of the scalar partners of the fermions m_0, and the mixing parameter of the two Higgs field doublets μ and $\tan\beta$ which is the ratio of the vacuum expectation values associated to the neutral Higgs bosons (h and A). Values around $\tan\beta = 1.5$ and 35 are favored by cosmological arguments.

7.1 Chargino Search

Pair production of charginos, the superposition of the fermionic W partners (winos) and the charged Higgs (higgsino), in e^+e^- collision as predicted by the MSSM is depicted in Fig. **??**. Two diagrams contribute: s-channel boson exchange and t-channel exchange of a sneutrino, $\tilde{\nu}$, the massive supersymmetric partner of the neutrino. For most of the parameter space usually considered, these two diagrams interfere destructively such that predicted cross sections are generally higher if a large mass for the sneutrino is assumed.[?]

Expected cross sections at LEP 1.5 energies for chargino pair production as a function of the chargino mass are shown in Fig. **??** (Ref.[?]). The two plots correspond to a very high sneutrino mass and to a light $\tilde{\nu}$ compatible with the

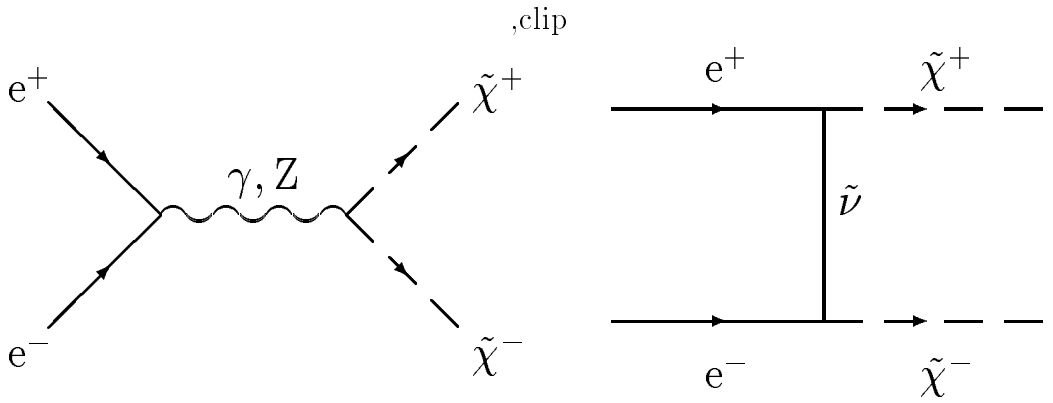

Figure 24: Feynman diagrams contributing to SUSY chargino pair production.

lower bounds obtained at LEP I. The parameters of the MSSM are varied in the range $0 < M_2 < 800$ GeV, $-400 < \mu < 400$ GeV and $\tan\beta = 1,\ 1.5,\ 35$. In addition, the chargino is assumed to be at least 10 GeV heavier than the neutralino. Under these assumptions, cross sections in the $\mathcal{O}$(pb) are expected (Fig. **??**) and a luminosity of a few inverse picobarn at high energy would allow the discovery of the chargino or to push the mass limits beyond the LEP I range.

The chargino is assumed to decay via W radiation into a neutralino, $\tilde{\chi}_1^0$, the lightest SUSY particle which interacts only weakly and hence escapes the detector undetected (Fig. **??**). The signature of chargino production is thus missing energy from the $\tilde{\chi}_1^0$, and eventually the neutrino from the W decay, and the decay products of the two W's: an acoplanar lepton pair, two jets, and an isolated lepton or acoplanar jets with missing energy.

In addition to the background at lower energies, fermion pair production and two-photon collisions, new important background sources for SUSY searches, play a role at $\sqrt{s} = 161$ GeV. W pairs with one of the bosons decaying leptonically have similar signatures as charginos. Also, single W production, as depicted in Fig. **??**, with the electron escaping through the beam pipe can fake SUSY signature. Figure **??** shows one candidate found by L3 in the search for SUSY at 161 GeV, which can be explained in the SM by single W production. For a total luminosity of 5.5 pb^{-1} analyzed at the time of the conference, this was the only candidate event found with 1.9 background events from SM processes expected. The new background sources require more stringent experimental cuts and hence reduce efficiency for the SUSY signal.

The data between 130 and 161 GeV show no evidence for SUSY. The results

,clip

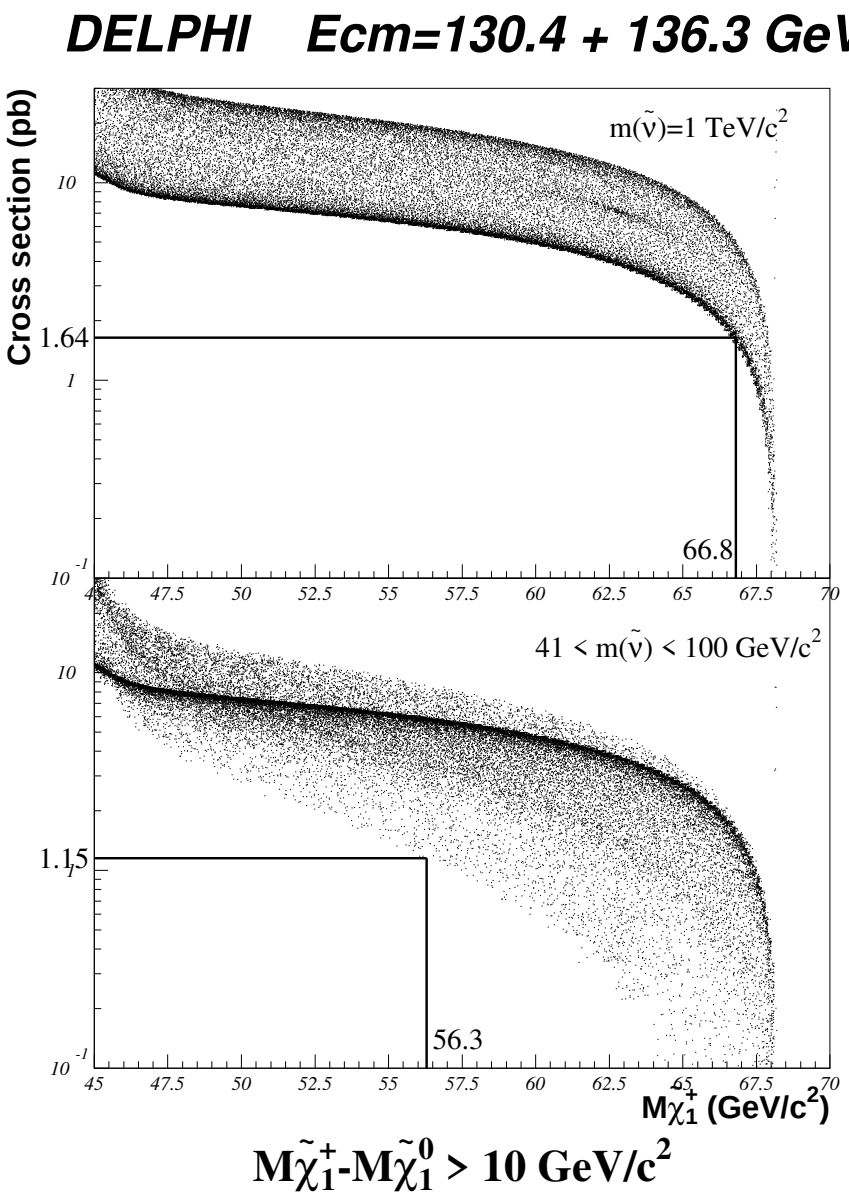

Figure 25: Expected cross sections for chargino pair production as a function of the chargino mass.

Figure 3: Scatter plot of the expected cross-section at 136.3 GeV versus the chargino mass in the non-degenerate scenario ($\Delta M > 10$ GeV/c^2). The MSSM parameters M and μ have been varied in the ranges $0 < M < 800$ GeV/c^2 and –400 GeV/c^2 $< \mu <$ 400 GeV/c^2 for three different values of $\tan\beta$: 1, 1.5 and 35. A very heavy sneutrino ($m_{\tilde{\nu}}$= 1 TeV/c^2) has been assumed in the upper part and a light sneutrino (41 GeV/c^2 $< m_{\tilde{\nu}} <$ 100 GeV/c^2) in the lower one.

,clip

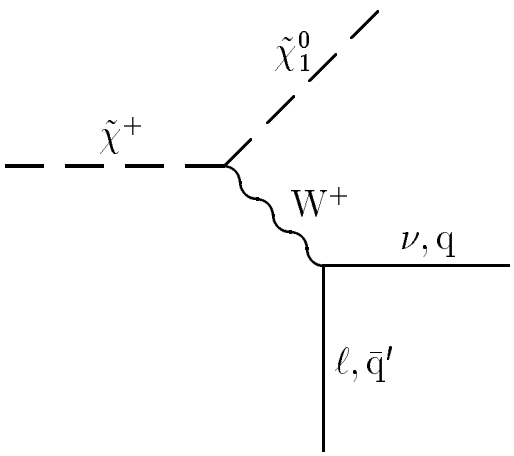

Figure 26: Chargino decay into the lightest neutralino and a W boson.

,clip

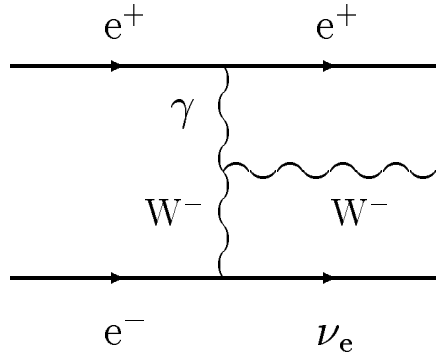

Figure 27: Single W production $\mathrm{e^+e^-} \to \mathrm{W^-e^+}\nu_{\mathrm{e}}$ at LEP II.

,clip

Candidate event

Run # **658610** **Event #** **4074** Total Energy : 78.44 GeV

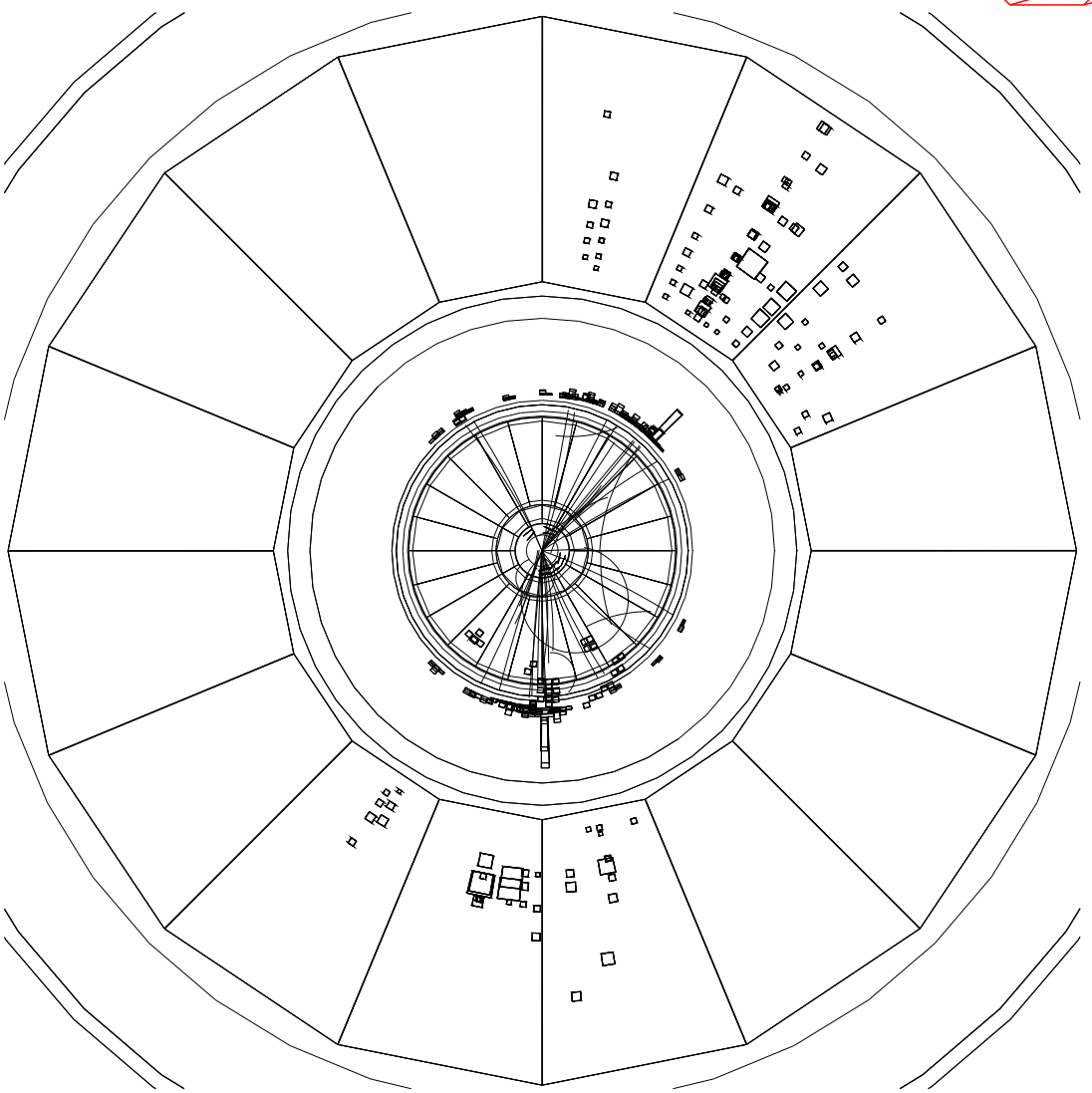

Possible explanation:

$$e^+e^- \rightarrow \quad We\nu_e$$

$$W \rightarrow \quad qq^{'}$$

can be converted into experimental upper limits on cross sections. As an example, Fig. ?? shows the experimental upper limit on the cross section $e^+e^- \to \tilde{\chi}^+\tilde{\chi}^-$ at 161 GeV obtained by ALEPH. The plot shows the range of $\tilde{\chi}^\pm$ masses not explored at LEP I. The results of LEP 1.5 are included in the plot by applying appropriate phase space factors. The shaded area is excluded kinematically and by requiring that the neutralino is lighter than the chargino.

A low cross section ($\sigma_{\tilde{\chi}^+\tilde{\chi}^-} \leq 0.7$ pb) is excluded in the region $m_{\tilde{\chi}^\pm} \approx 50$ GeV and $m_{\tilde{\chi}^0} \approx 20$ GeV where the kinematic conditions are favorable providing high detection efficiency and good background suppression. Limits on the cross section become worse as the neutralino mass approaches the mass of the chargino because the visible energy in the detector becomes lower and thus reduces the detection efficiency. Also, background from two photon processes is larger there. Similarly, if the mass difference between the chargino and neutralino becomes large, the missing energy is reduced and chargino events resemble more and more ordinary fermion pairs. This makes background suppression difficult, and consequently, only higher cross sections can be excluded.

This type of presenting search results is less model dependent as it makes only assumptions about the decay of SUSY particles, e.g., the chargino decay in Fig. ??, which is needed for the calculation of detection efficiencies. For the interpretation in terms of limits on SUSY parameters, like the chargino mass, one calculates chargino pair cross sections for different sets of SUSY parameters and compares them to the experimental cross section limit as shown in Fig. ??. The exclusion limit on the chargino mass is only valid in the range of SUSY parameters considered. Figure ?? shows the exclusion in the $m_{\tilde{\chi}^\pm} - m_{\tilde{\chi}^0}$ plane obtained by DELPHI at LEP 1.5 using the calculated cross sections shown in Fig. ?? and the parameter space considered there. With the assumption of a heavy sneutrino, chargino masses close to the kinematic limit can be ruled out.

7.2 Neutralino Search

The MSSM predicts the existence of four weakly interacting neutralinos $\tilde{\chi}_i^0$ with the index i ordering them by mass. Assuming R parity conservation and following cosmological arguments, the lightest neutralino, $\tilde{\chi}_1^0$, must be stable and invisible.

The production of a pair of kinematically allowed, but not necessarily identical,

neutralinos in e^+e^- annihilation is depicted in Fig. **??**. The decay of a heavier neutralino into $\tilde{\chi}_1^0$ proceeds by radiation of a Z and thus giving rise to missing energy and a pair of jets or leptons (Fig. **??**). The decay through photon radiation is also possible and has been searched for.[?]

The non-observation of a signal can be expressed in terms of cross-section limits on neutralino production. Similar to Fig. **??**, the experimental upper limit of the cross section $e^+e^- \to \tilde{\chi}_2^0 \tilde{\chi}_1^0$ at $\sqrt{s} = 161$ GeV as a function of the masses of the two lightest neutralinos is shown in Fig. **??**.

Again interpretation in terms of SUSY parameters requires more assumptions about the model. The cross section limits on neutralino pair production can be interpreted in terms of mass limits for the right-handed supersymmetric partner of the electron, $\tilde{e}_R$. Figure **??** shows the L3 result from LEP 1.5 assuming MSSM parameters in the range $0 < M_2 < 200$ GeV, $-200 < \mu < 200$ GeV, and $\tan\beta = 1$. The high-energy data enlarge the excluded region in the $m_{\tilde{e}_R} - m_{\tilde{\chi}_1^0}$ plane as compared to the limits obtained at LEP I owing to the relatively high sensitivity due to the t-channel contribution to neutralino pair production (Fig. **??**).

For the other bosonic partners of the SM fermions, the LEP I limits are not improved. From a combined analysis of the data taken at the Z resonance and at $130 - -140$ GeV, the ALEPH collaboration sets a lower mass limit for the lightest neutralino $m_{\tilde{\chi}_1^0} > 12.8$ GeV (Ref.[?]).

The results on SUSY searches are often presented in an exclusion plot for the μ and M_2 parameters. Figure **??** shows the result obtained by OPAL using about 3 pb^{-1} at 161 GeV and including those regions already excluded at LEP I and LEP 1.5. The two plots are obtained assuming two different values for $\tan\beta$ and the mass scale for the scalar partners of the fermions to be $m_0 = 1$ TeV.

8 Four-Jet Events at $\sqrt{s} \geq 130$ GeV

A detailed study of four-jet hadronic events at LEP 1.5 has been reported by the ALEPH Collaboration.[?] From selected four-jet events, the invariant masses of jet pairs are computed, and out of the three jet combinations, the one with the lowest difference in jet-pair masses is retained. The distribution of the sum of these two jet-pair masses is shown in Fig. **??**. Not only the total number of four-jet events observed by ALEPH at $130 - -140$ GeV is larger than expected from QCD, but this excess is contained in a narrow window around 105 GeV for

the sum of the jet-pair masses. In this window, about two times the estimated resolution wide, nine events are observed with only 0.8 events expected from QCD. Detailed discussion of this observation can be found in Ref..[?]

Similar analyses have been performed by the other three LEP experiments on their LEP 1.5 data, and all find agreement with the QCD expectation.[?,?] No anomaly neither in the total four-jet rate nor in the jet-pair mass distribution is seen by any of the other experiments. Combining the four LEP experiments, one obtains the distribution shown in Fig. ?? (Ref.[?]). However, with the limited statistics, a possible signal cannot be ruled out. By averaging the four experiments, a cross section for four-jet events with the sum of the jet-pair mass equaling 105 GeV can be derived:[?]

$$\sigma(\Sigma\, m_{ij} = 105\ \mathrm{GeV}) = 1.2 \pm 0.4\ \mathrm{pb}\,. \tag{14}$$

Neutral SUSY Higgs boson production $\mathrm{e^+e^-} \to \mathrm{h\,A}$ is not likely to explain the surplus of four-jet events at $\sum m_{ij} = 105$ GeV, as the expected cross section is much lower and there is no evidence for b-quark enrichment in the nine ALEPH events. The latter argument would not apply for charged SUSY Higgs boson $\mathrm{e^+e^-} \to \mathrm{H^+\,H^-} \to \mathrm{c\bar{s}\,\bar{c}s}$, but in this case, $\mathrm{c\bar{s}}\,\tau^-\bar{\nu}_\tau$ final states should also be observed. Clarification of the ALEPH observation is expected from more luminosity at energies $\sqrt{s} \geq 130$ GeV. The first results reported from the 161 GeV run are in agreement with the SM expectation.[?]

9 Studies of Photon Final States

Every time a new energy domain is experimentally accessible, studies of events with hard photons draw much attention since many extensions of the SM predict significant additional sources of photon production. Compositeness of SM particles is just one example. The studies of single and multiphoton final states at LEP 1.5 are described in Refs..[?,?,?,?]

Single-photon final states have been used at LEP I to determine the number of light neutrino generations (Fig. ??). At energies above the Z pole, the energy spectrum of the observed photon is very much different since the return to the Z gives rise to very energetic photons. Figure ?? shows the spectrum measured by the L3 experiment at 161 GeV. One clearly sees the peak at $E_\gamma = 55$ GeV which is just the energy of the ISR photon which leaves $\sqrt{s'} = m_\mathrm{Z}$ for the annihilating

e^+e^- system. The rate and the energy distribution of the single photon events are in good agreement with the SM expectation.

Two-photon final states in the reaction $e^+e^- \to \gamma\gamma$ are mediated by t-channel exchange of an electron. The reaction can be used to test the point-like structure of electrons because the existence of an excited electron, e^*, would lead to a different angular distribution of the photons. Deviations from QED are parametrized by two cutoff parameters $\Lambda_\pm$

$$\frac{d\sigma}{d\Omega} = \left(\frac{d\sigma}{d\Omega}\right)_{QED} \left(1 \pm \frac{s^2}{2\,\Lambda_\pm^4}\left(1 - \cos^2\Theta^*\right), \right) \tag{15}$$

with Θ^* being the scattering angle in the two-photon rest frame. As an example, Fig. ?? shows the result obtained by ALEPH at LEP 1.5. The plot shows the ratio of measured to QED differential cross section as a function of the scattering angle. Good agreement is observed, and 95% C.L. limits of the cutoff parameters of 132 and 169 GeV, respectively, are derived.

No deviation from QED in this reaction has yet been reported from the data at $\sqrt{s} = 161$ GeV which would allow us to further increase the limits on $\Lambda_\pm$ by about 30 GeV.

10 Search for Excited and Heavy Leptons

The LEP experiments have searched for excited states of the known fundamental charged and neutral leptons, e^*, μ^*, τ^*, and ν^*. Excited leptons can be produced either in pairs ($e^+e^- \to \ell^*\ell^*$) or singly ($e^+e^- \to \ell\ell^*$). As the excited leptons are thought to decay radiatively into their ground states, their existence would lead to anomalies in the observed $\ell^+\ell^-\gamma$ and $\ell^+\ell^-\gamma\gamma$ final states. If produced in pairs, the expected cross section is, apart from kinematic suppression, assumed to be the same as for ordinary lepton pairs. Therefore, excited leptons can be excluded up to the kinematic limit of $m_{\ell^*} \approx E_b$ with a relatively small luminosity. In principle, exclusion up to $m_{\ell^*} \approx \sqrt{s}$ can be achieved from single ℓ^* production. This, however, depends on assumptions on coupling constants.

The decay of excited leptons through Z and W radiation has also been investigated. Details of the analysis at LEP 1.5 can be found in Refs..[?,?,?,?] As an example, the excluded mass of a charged excited lepton as a function of the coupling parameter λ is shown in Fig. ?? as obtained at LEP 1.5 by ALEPH.

The precision measurements of Z parameters at LEP have shown that there are only the three fermion generations with light neutrinos ($m_\nu < m_{\rm Z}/2$). However, there still could exist a fourth generation with all fermions being heavy. Searches for neutral ($\rm L^0$) and charged ($\rm L^\pm$) heavy leptons are performed at LEP. These particles are assumed to be produced in pairs, and they decay through W radiation into known fermions: $\rm L^0 \to \ell^\pm W^\mp$ and $\rm L^\pm \to \nu_L W^\pm$. No sign for these new particles has been observed so far. Details can be found in Refs..[?,?,?] Figure ?? shows the result of OPAL at LEP 1.5 in the mass plane of the charged and neutral heavy lepton.

11 Conclusions

The second phase of the LEP program has started in October 1995 with cms energies of $130 - -140$ GeV, and it continued in June 1996 at $\sqrt{s} = 161$ GeV at the $\rm e^+e^- \to W^+W^-$ threshold. The energy upgrade was successful, and good luminosity and background conditions were provided to the experiments.

From the measured cross section at the threshold using the first part of the 161 GeV data, the LEP experiments determine the mass of the W boson to be

$$m_{\rm W} = 80.4 \pm 0.3 \pm 0.1({\rm LEP})\ {\rm GeV},$$

in excellent agreement with the value measured at $\rm p\bar{p}$ colliders and the mass derived from precise measurement of electroweak corrections at the Z pole.

For the first time, fermion pair production in $\rm e^+e^-$ annihilation has been studied above the Z resonance. This provides a much improved determination of the γZ interference as compared to the LEP I data.

The search for new physics has been extended into a new energy regime. No sign of Supersymmetry has been observed at LEP, and lower mass limits have been improved, in particular, for the chargino.

The Standard Model of electroweak and strong interactions is confirmed up to an energy of 161 GeV.

The energy of LEP will be further increased in steps up to $\sqrt{s} = 192$ GeV with the goal of collecting 500 $\rm pb^{-1}$ per experiment, which will allow us the determination of W parameters and to extend the search for new particles, in particular, for the Higgs boson up to $m_{\rm H} \approx 100$ GeV.

12 Acknowledgments

I would like to thank my colleagues from the LEP experiments for providing preliminary results from the recent run. In particular, I am grateful to A. Blondel, D. Charlton, R. Faccini, M. Grünewald, S. Mele, C. Paus, M. Schmitt, U. Uwer, and G. Wilkinson for their help in preparing my talk. I thank A. Böhm and S. Wynhoff for the careful reading of the manuscript.

,clip

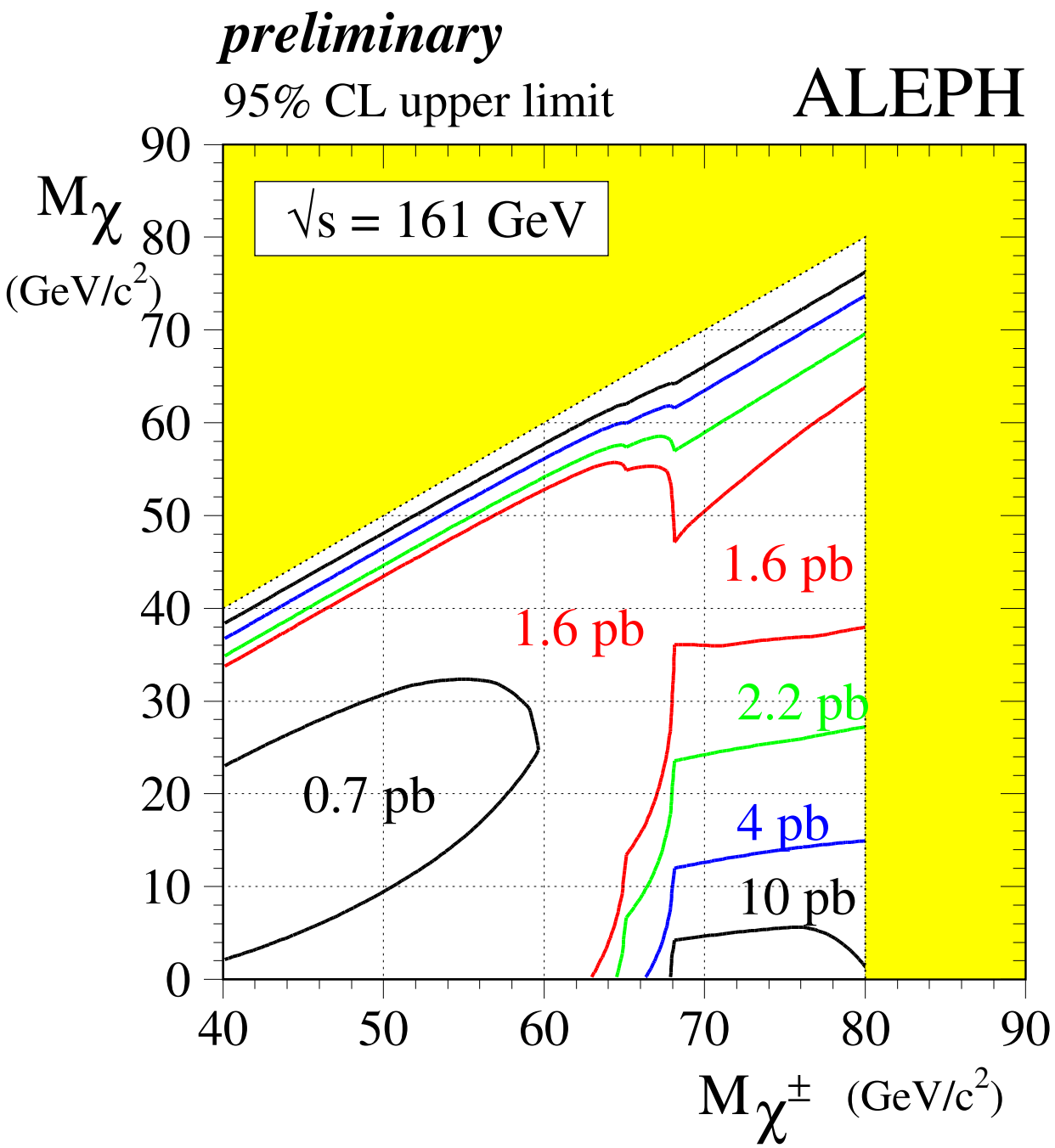

Figure 29: Experimental upper limits (95% C.L.) on the cross section $e^+e^- \to \tilde{\chi}^+\tilde{\chi}^-$ at $\sqrt{s} = 161$ GeV in the mass plane of the chargino and the lightest neutralino, here denoted χ, obtained by ALEPH. The shaded area is kinematically excluded and the remaining area is subdivided into five regions with different experimental upper cross-section limits.

,clip

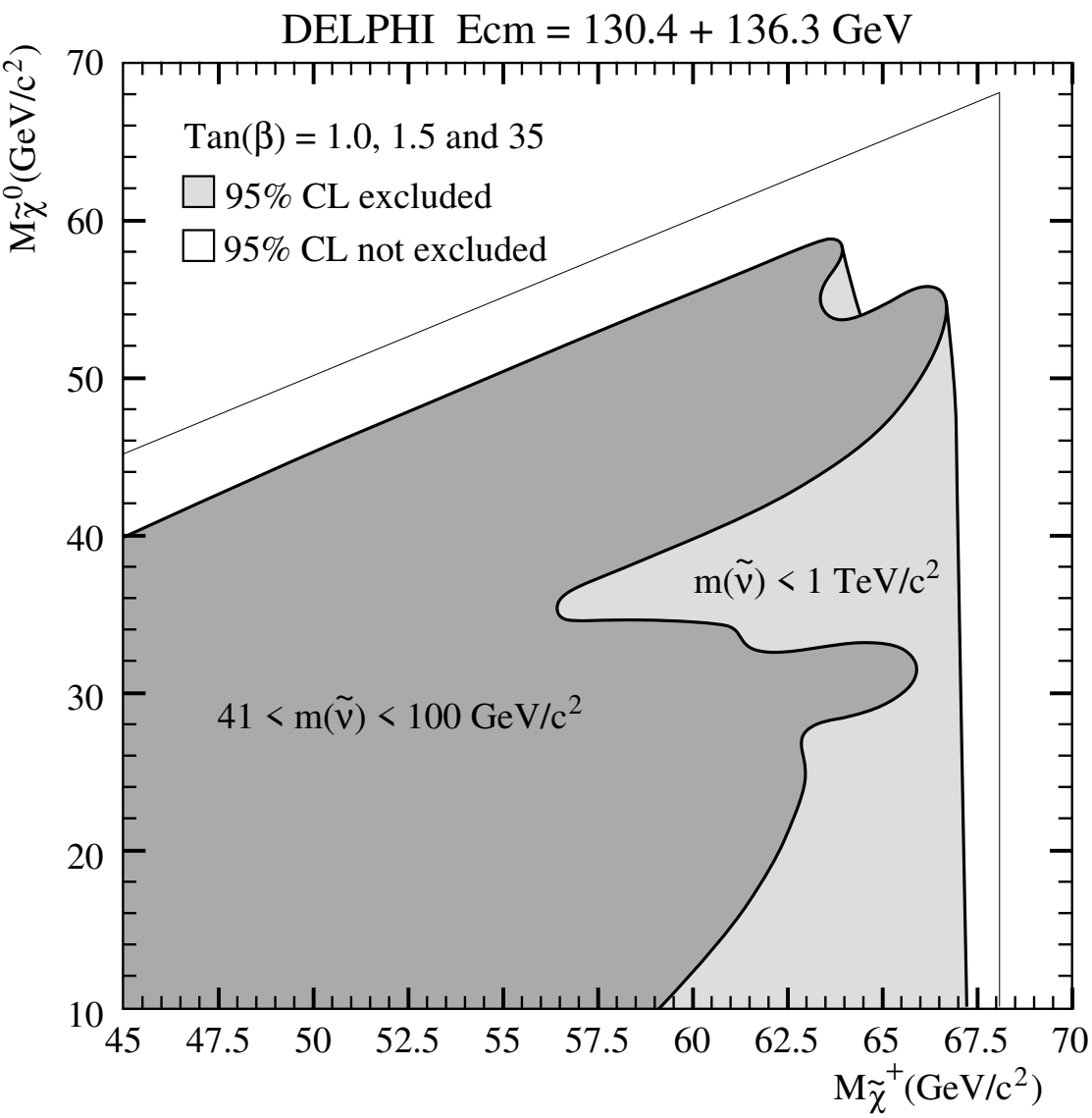

Figure 30: Limits set by DELPHI on the chargino mass from LEP 1.5 shown in the $m_{\tilde{\chi}^{\pm}} - m_{\tilde{\chi}^0}$ plane.?

Figure 5: Regions excluded at the 95% C.L. in the ($m_{\tilde{\chi}_1^{\pm}}$, $m_{\tilde{\chi}_1^0}$) plane. Three different values of $tan\,\beta$ have been used: 1, 1.5 and 35. The regions excluded when the sneutrino is light (41 GeV/c^2 $< m_{\tilde{\nu}} <$ 100 GeV/c^2) are shown in dark grey; the additional regions excluded when the sneutrino is very heavy ($m_{\tilde{\nu}} = 1$ TeV/c^2) are shown in light grey. The outermost line corresponds to the kinematic limit.

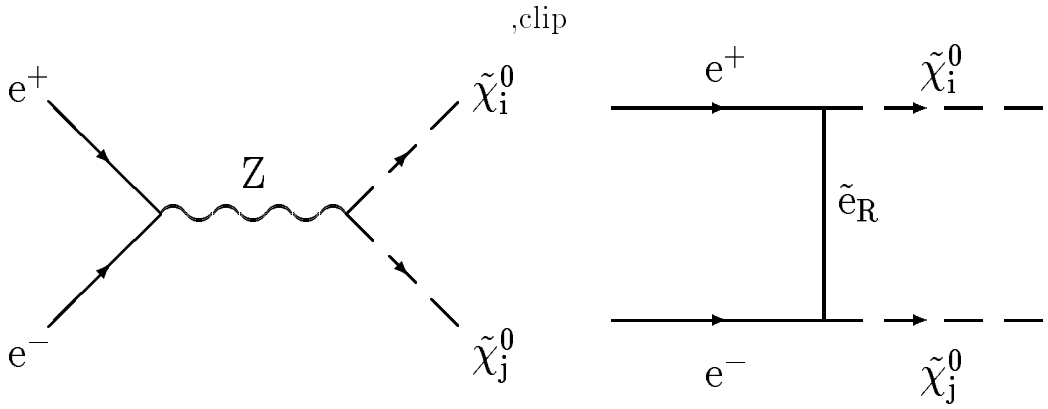

Figure 31: Feynman diagrams contributing to SUSY neutralino pair production.

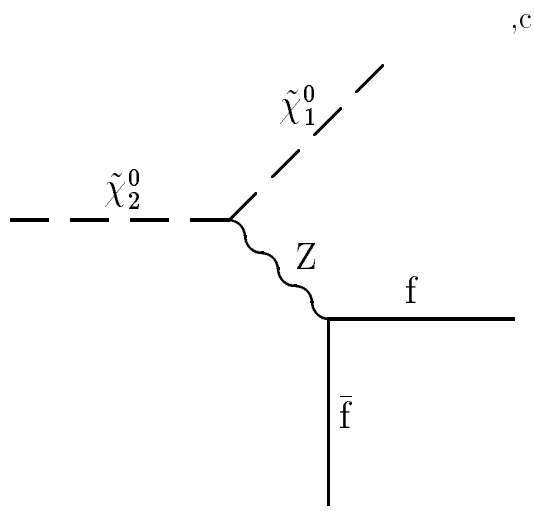

Figure 32: Decay of the second lightest into the lightest neutralino by radiating a Z boson.

,clip

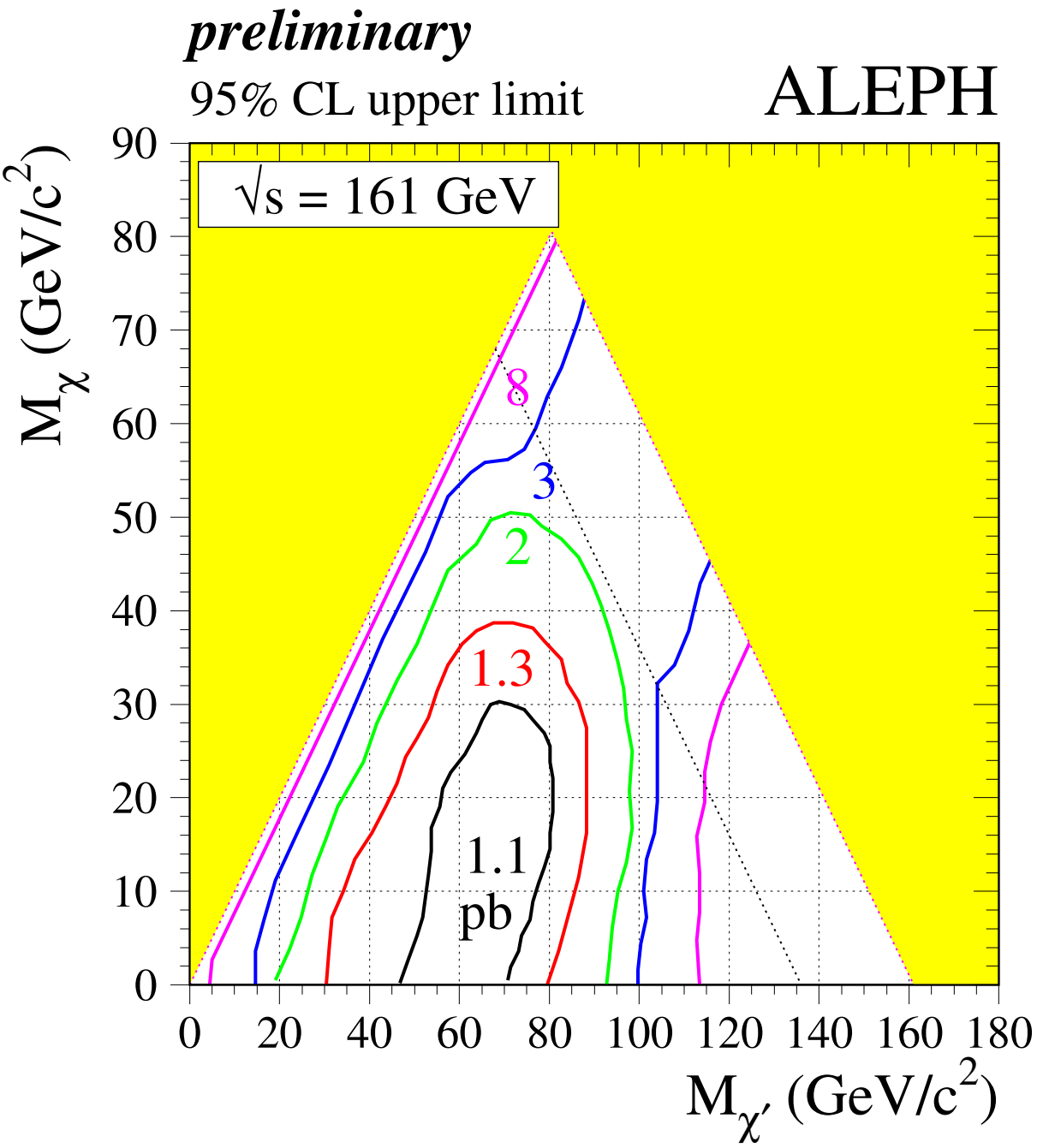

Figure 33: Same as Fig. ?? for the cross section $e^+e^- \to \tilde{\chi}_2^0 \tilde{\chi}_1^0$ (here labeled χ' and χ).

,clip

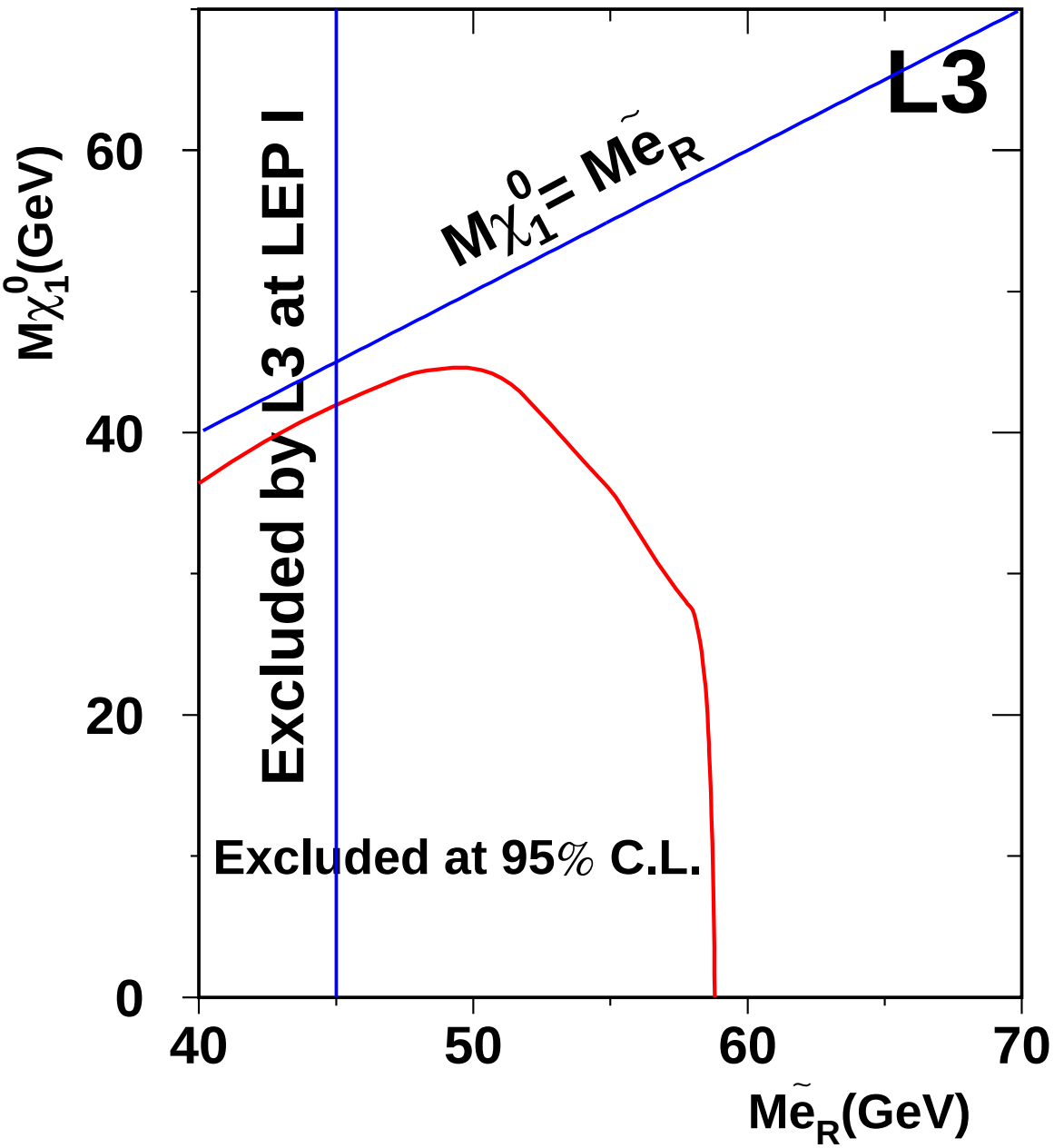

Figure 34: Mass limit for the right-handed supersymmetric partner of the electron in the mass plane obtained at LEP 1.5 compared to LEP I result.

Figure 6: Excluded region, in the $M_{\tilde{e}_R} - M_{\tilde{\chi}_1^0}$ plane, with $\tan\beta = 1.5$ and for any values of the parameters in the ranges $0 < M_1 < 200$ GeV, $-200 < \mu < 0$ GeV and $0 < m_0 < 100$ GeV.

,clip

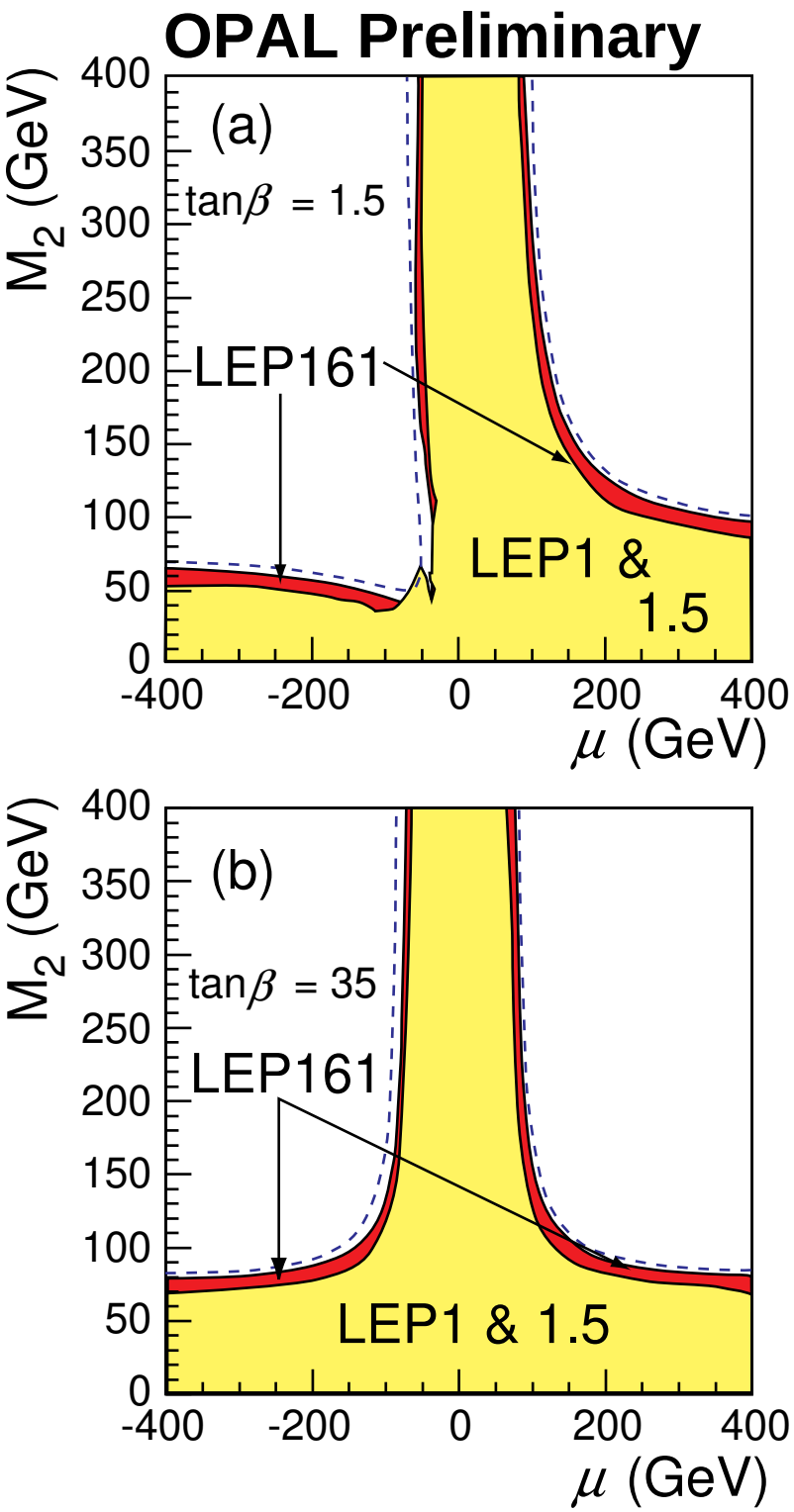

Figure 35: Exclusion (95% C.L.) of SUSY parameters μ and M_2 for two different values of $\tan\beta$ and for $m_0 = 1$ TeV from OPAL. The limits obtained from 161 GeV are compared to the combined limits from LEP I and LEP 1.5. The broken lines indicate the kinematic limit at 161 GeV for chargino pair production.

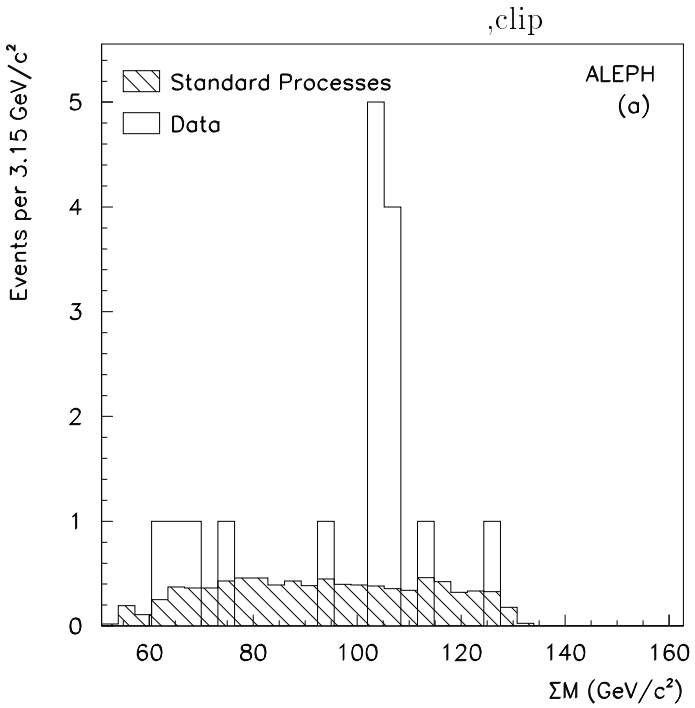

Figure 36: Sum of jet-pair masses in four-jet hadronic events as observed by ALEPH for cms energies of $130 - -140$ GeV.

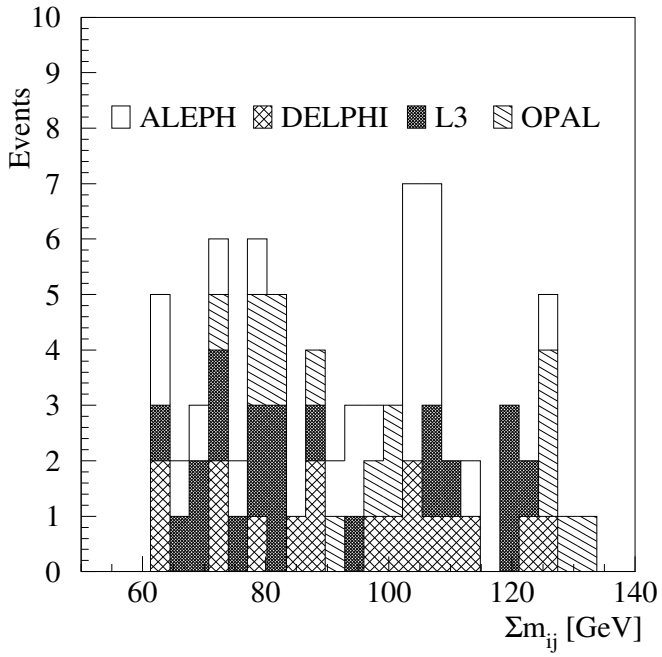

Figure 37: Distribution of the sum of jet-pair masses in four-jet hadronic events as observed by the four LEP experiments at cms energies of $130 - -140$ GeV.

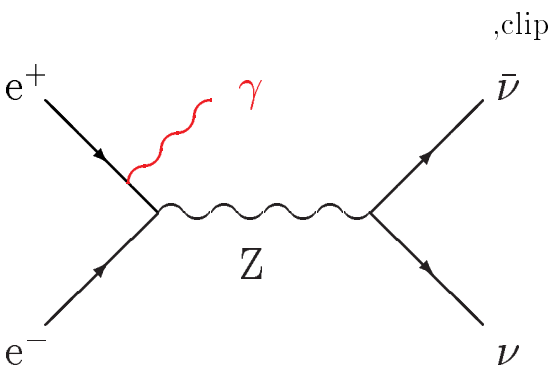

Figure 38: Feynman diagram contributing to the single photon reaction in the SM.

Single photon events

$\sqrt{s} = 161$ **GeV**

$\mathcal{L}_{int} = 6.5 pb^{-1}$

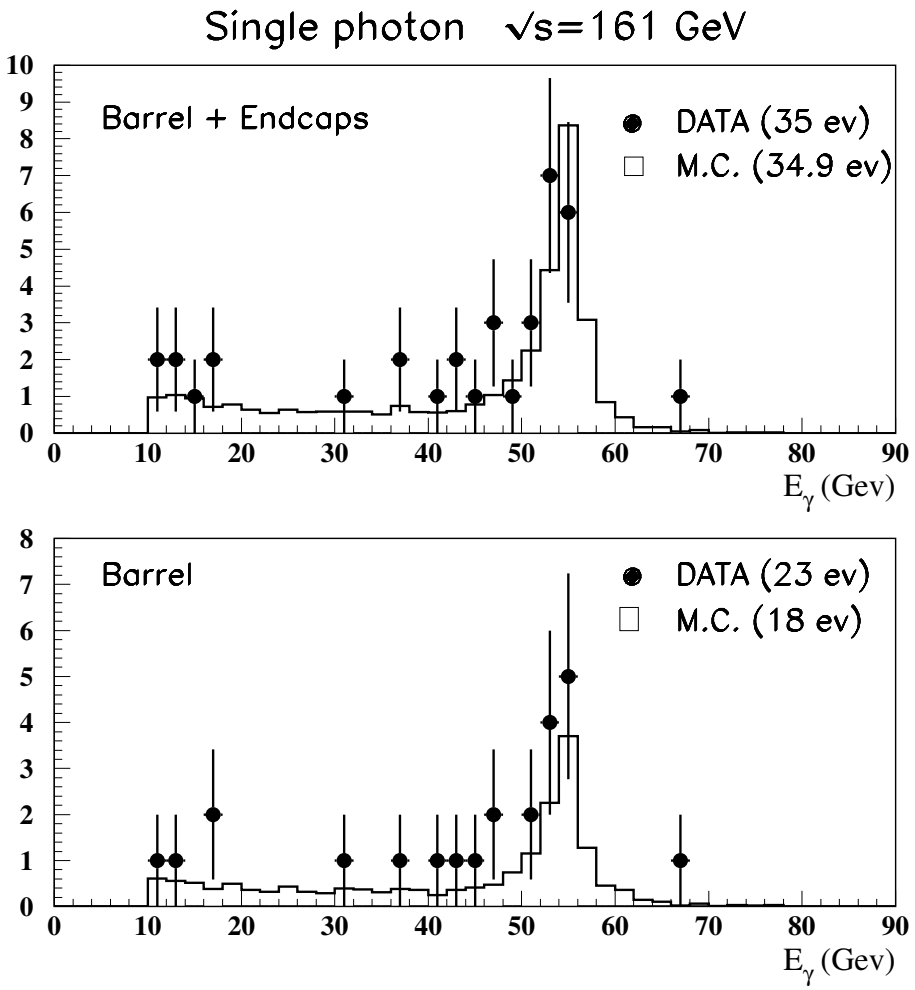

Figure 39: Spectrum of single photon events observed by L3 at $\sqrt{s} = 161$ GeV. The top plot shows the total sample and the bottom plot the events at large polar angles ($44° \leq \Theta \leq 136°$). The points are the data, and the histograms show the SM expectations.

,clip

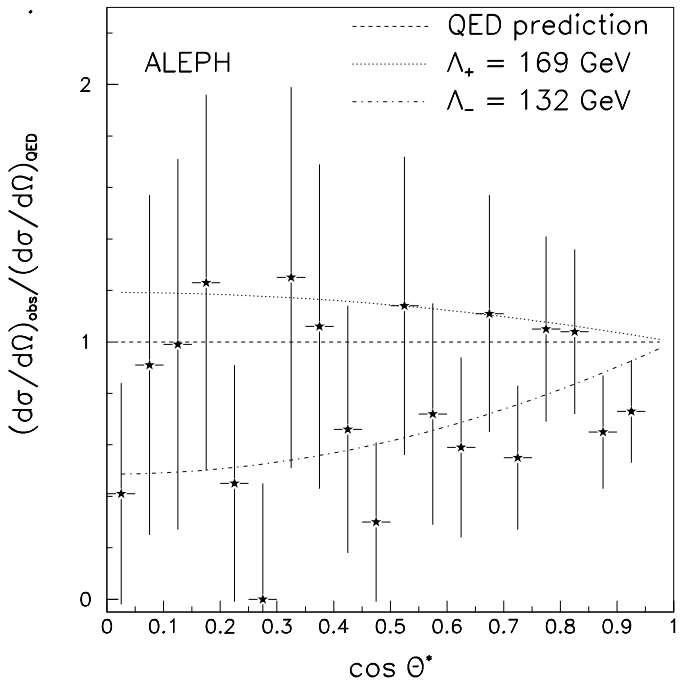

Figure 3: The ratio of the observed to predicted cross sections for the process $e^+e^- \to \gamma\gamma(\gamma)$ as a function of $\cos\theta^*$. Also shown are the 95% confidence level limits on the QED cut-off model.

Figure 40: Ratio of the experimental and QED expected differential cross section of the reaction $e^+e^- \to \gamma\gamma$ as measured by ALEPH at cms energies between 130 and 140 GeV(Ref.?). The two lines show the maximum deviation experimentally allowed according to the parametrization of Eq. ?? from which limits for $\Lambda_\pm$ are derived.

If two-electron, two-photon contact interactions exist, then the cross section for two-photon production becomes

$$\frac{\mathrm{d}\sigma}{\mathrm{d}\Omega} = \left(\frac{\mathrm{d}\sigma}{\mathrm{d}\Omega}\right)_{\mathrm{QED}} + \left(\frac{\mathrm{d}\sigma}{\mathrm{d}\Omega}\right)_{\mathrm{contact}},$$

where the second term includes both the contact interactions themselves and their interference term with QED (which is usually a larger effect). The exact form of the cross section depends on the chirality of the electron current that can take part in the interaction, leading to the possibility of left (L), right (R), L+R and L−R amplitudes. The expressions for the cross sections are given in [8] and [10].

A fit was performed in exactly the same way as for the simple QED cut-off model, with $\epsilon = \Lambda^{-4}$ except in the L−R case where the interference term vanishes and the lowest order dependence on Λ is Λ^{-8}. For this model, the fit was performed in Λ^{-8}, and the sensitivity is seen to be reduced. The results are shown in Table 3. An alternative description of extensions to QED is provided by considering non-standard effective Lagrangians containing operators of dimensions 6, 7 or 8 [20]. Making the same assumptions as the authors of Ref. [20] that $\Lambda = \tilde{\Lambda} \equiv \Lambda_6$, $\Lambda_S = \Lambda_P \equiv \Lambda_7$ and $\Lambda_A \equiv \Lambda_8$, the above procedure yields the following 95% confidence limits: $\Lambda_6 > 676\,\mathrm{GeV}$,

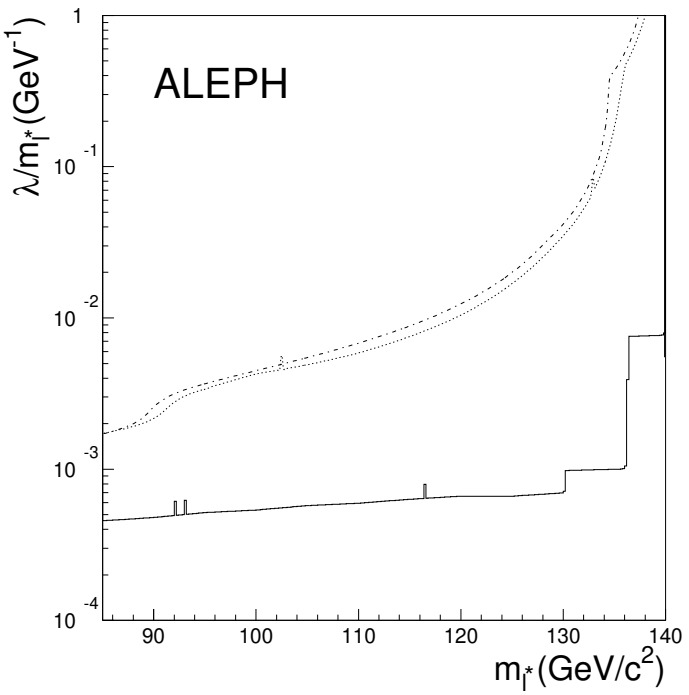

0.9

Figure 41: Exclusion limits (95% C.L.) in the mass-coupling plane for singly produced charged leptons ℓ^* as obtained by ALEPH at LEP 1.5. The solid, dotted, and dot-dashed lines are for e^*, μ^*, and τ^*, respectively.?

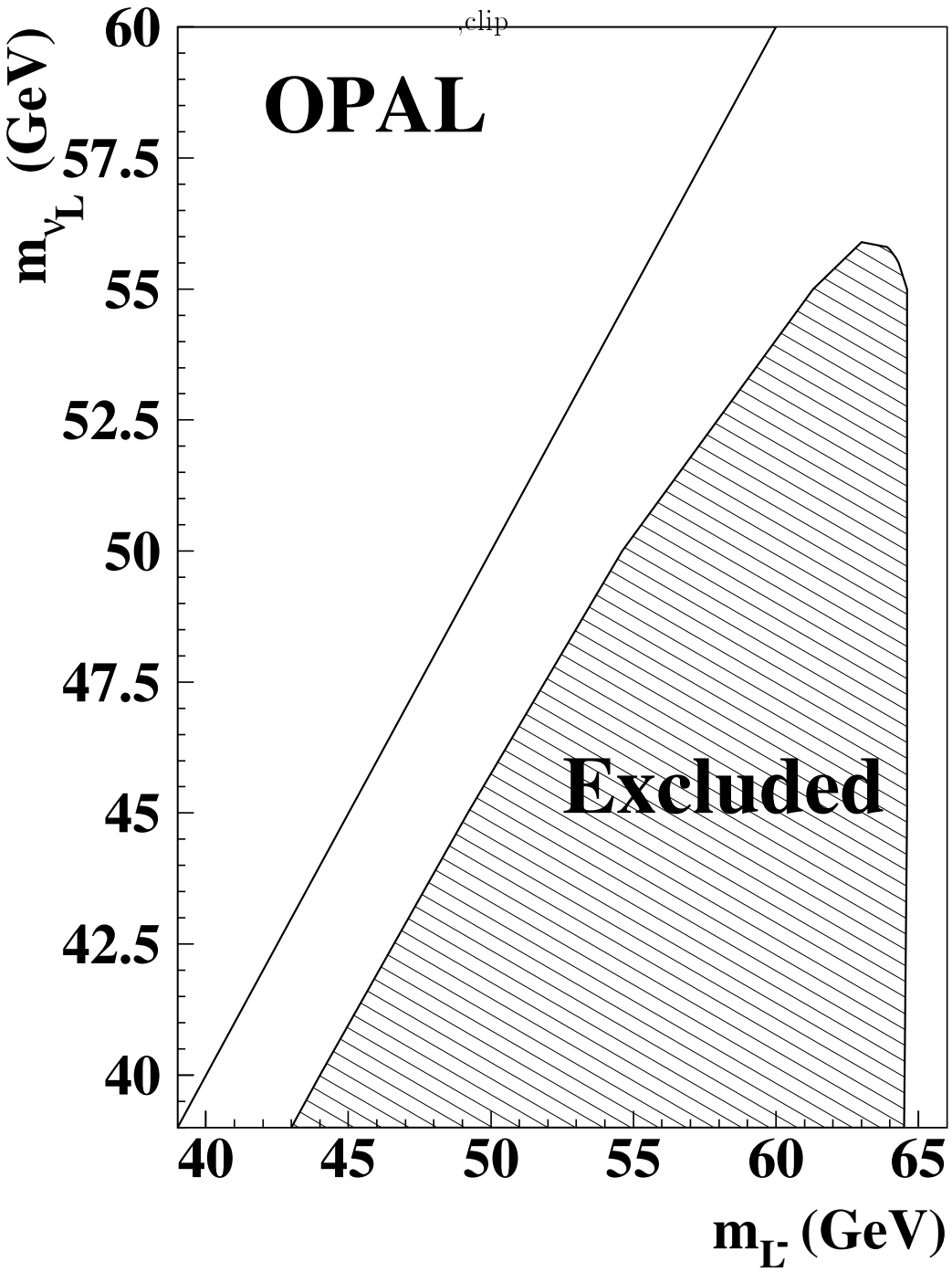

Figure 4: The excluded region in this analysis in the (m_{L^-}, $m_{\nu_{\mathrm{L}}}$) plane for case (B). If L^- decays into $\nu_{\mathrm{L}} + \mathrm{W}^-$ and ν_{L} is assumed to be a stable heavy neutrino, the hatched region is excluded with more than 95% C.L. The region $m_{\nu_{\mathrm{L}}} < 45$ GeV is already excluded for the Dirac ν_{L} and $m_{\nu_{\mathrm{L}}} < 39.5$ GeV for the Majorana ν_{L} from the upper limit of the Z^0 decay width measurements at LEP [3]. The diagonal line shows $m_{\mathrm{L}^-} = m_{\nu_{\mathrm{L}}}$.

Figure 42: The excluded region (95% C.L.) in the mass plane of the charged and neutral heavy leptons. The neutral heavy lepton is assumed to be stable.